



HAL
open science

Optimized global-in-time Schwarz algorithm for diffusion equations with discontinuous and spatially variable coefficients

Florian Lemarié, Laurent Debreu, Eric Blayo

► **To cite this version:**

Florian Lemarié, Laurent Debreu, Eric Blayo. Optimized global-in-time Schwarz algorithm for diffusion equations with discontinuous and spatially variable coefficients. [Research Report] RR-6663, INRIA. 2008, pp.45. inria-00324533

HAL Id: inria-00324533

<https://inria.hal.science/inria-00324533>

Submitted on 25 Sep 2008

HAL is a multi-disciplinary open access archive for the deposit and dissemination of scientific research documents, whether they are published or not. The documents may come from teaching and research institutions in France or abroad, or from public or private research centers.

L'archive ouverte pluridisciplinaire **HAL**, est destinée au dépôt et à la diffusion de documents scientifiques de niveau recherche, publiés ou non, émanant des établissements d'enseignement et de recherche français ou étrangers, des laboratoires publics ou privés.



INSTITUT NATIONAL DE RECHERCHE EN INFORMATIQUE ET EN AUTOMATIQUE

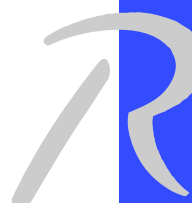
*Optimized global-in-time Schwarz algorithm for
diffusion equations with discontinuous and spatially
variable coefficients*

Florian Lemarié — Laurent Debreu — Eric Blayo

N° 6663

Octobre 2008

Thème NUM



R
rapport
de recherche

Optimized global-in-time Schwarz algorithm for diffusion equations with discontinuous and spatially variable coefficients

Florian Lemarié^{*†}, Laurent Debreu^{*†}, Eric Blayo^{*†}

Thème NUM — Systèmes numériques
Équipes-Projets MOISE

Rapport de recherche n° 6663 — Octobre 2008 — 45 pages

Abstract: In this report we present a global-in-time non-overlapping Schwarz method applied to the one dimensional unsteady diffusion equation. We address specifically the problem with discontinuous diffusion coefficients, our approach is therefore especially designed for subdomains with heterogeneous properties. We derive efficient interface conditions by solving analytically the minmax problem associated to the search of optimized conditions in a *Robin-Neumann* case and in a *two-sided Robin-Robin* case with constant coefficients. We study the impact of the finiteness of the subdomains on the optimized conditions. Then we address the problem with spatially variable coefficients. We derive a new approach to determine the convergence factor of the algorithm, which enables to optimize the convergence speed. The theoretical results are illustrated by numerical experiments in the case of *Robin-Robin* and *Dirichlet-Neumann* interface conditions.

Key-words: domain decomposition, waveform relaxation, Schwarz methods

* Jean Kuntzmann Laboratory, BP 53, 38041 Grenoble Cedex 9, France

† INRIA Grenoble Rhône-Alpes, Montbonnot, 38334 Saint Ismier Cedex, France

Algorithme de Schwarz optimisé global-en-temps pour des équations de diffusion à coefficients discontinus et spatialement variables

Résumé : Dans ce rapport nous présentons une méthode de Schwarz sans recouvrement globale en temps appliquée à l'équation de diffusion instationnaire 1D. Nous abordons spécifiquement le problème avec des coefficients de diffusion discontinus, notre approche est donc spécialement conçue pour des sous-domaines possédant des propriétés physiques hétérogènes. Nous dérivons des conditions d'interface efficaces en résolvant analytiquement le problème de min-max associé à la recherche de conditions optimisées dans un cas *Robin-Neumann* puis dans un cas *two-sided Robin-Robin* à coefficients constants. Nous étudions également l'impact de la taille des sous-domaines considérés sur les conditions optimisées. Ensuite nous abordons le problème avec des coefficients variables. Nous dérivons une nouvelle approche afin de déterminer le facteur de convergence de l'algorithme, ce qui nous permet d'optimiser la vitesse de convergence. Les résultats théoriques sont illustrés par des expériences numériques.

Mots-clés : décomposition de domaine, algorithmes de relaxation d'onde, méthodes de Schwarz

Part I

Introduction and model problem

1 Introduction

A number of geophysical phenomena, which may have a strong societal impact, involve the coupled ocean-atmosphere system (e.g. climate change, tropical cyclones...). It is therefore often necessary to couple numerical models of the ocean and of the atmosphere. However, connecting the two model solutions at the air-sea interface is a difficult problem, which is presently often addressed in a simplified way from a mathematical point of view. Indeed the fluxes exchanged by the two models are generally not in exact balance. This kind of coupling raises a number of challenges in terms of numerical simulation since we are considering two highly turbulent fluids with widely different scales in time and space. It is thus natural to use some specific numerical treatment to match the physics of the two fluids at their interface. It is known that, even if numerical models are much more complicated, a simple one-dimensional diffusion equation can locally satisfactorily approximate the main features of the flux exchanges between both fluids in the vertical direction. The corresponding diffusion coefficients are given by an *eddy-viscosity* closure which predicts strongly spatially variable diffusion coefficients, see [20]. Indeed in order to parameterize the effects of the boundary layers the turbulent diffusion term is defined (e.g. [23] [16]), with a large spatial variability to account for local effects. A parameterization with a constant diffusion, originally introduced in [6], is now known to be naive.

In order to perform this coupling in a more consistent way than *ad-hoc* methods, we propose to adapt a global-in-time domain decomposition based on optimized Schwarz method, described in [11] and designed thanks to the pioneering works [8] and [14], to our configuration with discontinuous and spatially variable coefficients. Indeed Schwarz-like domain decomposition methods provide flexible and efficient tools for coupling models with non-conforming time and space discretizations [3]. To circumvent the divergence of the classical Schwarz method in the case of non-overlapping subdomains, new transmission conditions of Robin type have been proposed in [18]. Then, thanks to the free parameters associated to the use of Robin conditions, an optimization of the convergence speed has been proposed in [9] and [14], which is the basis of the so called *optimized Schwarz methods* (OSM). This kind of method is based on the concept of absorbing boundary conditions [7]. It has been originally introduced for stationary problems and has been extended to unsteady cases by adapting the waveform relaxation algorithms (see [17] and [8]), to provide a *global-in-time optimized Schwarz method*. This notion of optimization of the convergence speed is critical in the context of ocean-atmosphere coupling as the numerical codes which are involved are very expensive from a computational point of view. We intend to derive interface conditions leading to an efficient Schwarz coupling algorithm between two unsteady diffusion equations. The convergence properties of this kind of problem have already been extensively studied in the case of a constant diffusion coefficient having the same value in all subdomains [10]. Moreover there exists a few results in the case of coefficients taking different constant values in the different subdomains [13] (in the more general case of

advection-diffusion-reaction equations). In the present papers, we extend these studies to the general case of diffusion coefficients which vary in each subdomain and which values are different on both sides of the interface.

In this report we first consider the case of diffusion coefficients which are constant in each medium, but discontinuous at their interface. We study a zeroth order *two-sided* optimized method by considering two different Robin conditions on both sides of the interface. In the second part the impact of the spatial variability in each medium of the diffusion coefficients on the convergence speed is studied.

This report is organized as follows. In this first part, we recall the basics of optimized Schwarz methods in the framework of time evolution problems. Then in the second part, sections 3 and 4 are dedicated to the study of two algorithms in the case of discontinuous but constant in each subdomain coefficients. In section 3 we determine the minimax problem solution for a simplified algorithm with only one Robin condition combined with a Neumann condition. In section 4, we address the more general case of *two-sided* optimized Robin-Robin transmission conditions, which are determined through a study of the behaviour of the convergence factor. In section 5 we extend our study of the convergence to a model problem with bounded subdomains. In the third part, we study the impact of the variability of the diffusion coefficients, in particular in the vicinity of the interface, on the convergence properties of the Schwarz algorithm. To our knowledge, the spatial variability of the coefficients has never been considered in the framework of Schwarz-like methods, except in [18] where absorbing conditions are given for the stationary case.

2 Model problem and Optimized Schwarz Methods

Our guiding example is the one dimensional diffusion equation

$$\mathcal{L}u = \partial_t u - \partial_x(D(x)\partial_x u) = f \quad \text{in } \Omega \times [0, T] \quad (2.1)$$

with $\Omega = [-L_1, L_2]$, $(L_1, L_2 \in \mathbb{R}^+)$ and $D(x) > 0, x \in \Omega$. This problem is complemented by an initial condition

$$u(x, 0) = u_0(x) \quad x \in \Omega, \quad (2.2)$$

and boundary conditions

$$\mathcal{B}_1 u(-L_1, t) = g_1 \quad \mathcal{B}_2 u(L_2, t) = g_2 \quad t \in [0, T]. \quad (2.3)$$

where \mathcal{B}_1 and \mathcal{B}_2 are partial differential operators.

In the whole paper we assume that $u_0 \in H^1(\Omega)$, $f \in L^2(0, T; L^2(\Omega))$, and $D(x)$ bounded in L^∞ -norm. Note that, in actual applications, such assumptions are generally fulfilled. Existence and uniqueness results for this problem can be proved following [13].

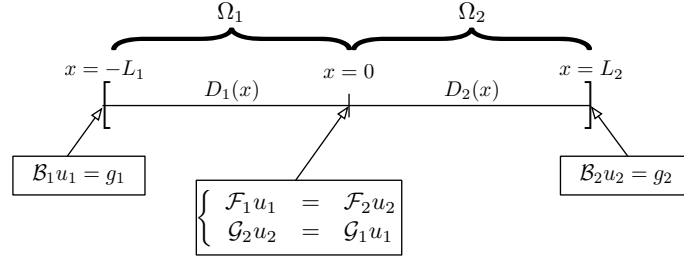


Figure 1: Decomposition of the spatial domain Ω into two non-overlapping subdomains.

2.1 Formulation of global-in-time Schwarz method

Let us now consider a case with discontinuous diffusion coefficients which could be representative of a coupling between media with heterogeneous physical properties. In this case each subdomain has its own diffusion profile $D_j(x)$, ($j = 1, 2$). This corresponds to a splitting of our domain Ω into two non-overlapping domains Ω_1 and Ω_2 (as described on figure 1) which communicates through their common interface $\Gamma = \{x = 0\}$ (note that there can be various reasons for such a splitting: different physics, parallelization and/or different numerical treatment requirements). The non-overlapping global-in-time Schwarz algorithm consists in solving iteratively subproblems on $\Omega_1 \times [0, T]$ and $\Omega_2 \times [0, T]$ using as an interface condition at $x = 0$ the corresponding values calculated at the previous iteration on the other subdomain. The operator \mathcal{L} defined previously is separated into two operators $\mathcal{L}_j = \partial_t - \partial_x(D_j(x)\partial_x)$ restricted to Ω_j ($j = 1, 2$). If we introduce the operators $\mathcal{F}_1, \mathcal{F}_2, \mathcal{G}_1$ and \mathcal{G}_2 to define the interface conditions, the algorithm reads

$$\left\{ \begin{array}{l} \mathcal{L}_1 u_1^k = f \\ u_1^k(x, 0) = u_o(x) \\ \mathcal{B}_1 u_1^k(-L_1, t) = g_1 \\ \mathcal{F}_1 u_1^k(0, t) = \mathcal{F}_2 u_2^{k-1}(0, t) \end{array} \right. \begin{array}{l} \text{in } \Omega_1 \times [0, T] \\ x \in \Omega_1 \\ t \in [0, T] \\ \text{in } \Gamma \times [0, T] \end{array} \quad \left\{ \begin{array}{l} \mathcal{L}_2 u_2^k = f \\ u_2^k(x, 0) = u_o(x) \\ \mathcal{B}_2 u_2^k(L_2, t) = g_2 \\ \mathcal{G}_2 u_2^k(0, t) = \mathcal{G}_1 u_1^k(0, t) \end{array} \right. \begin{array}{l} \text{in } \Omega_2 \times [0, T] \\ x \in \Omega_2 \\ t \in [0, T] \\ \text{in } \Gamma \times [0, T] \end{array} \quad (2.4)$$

where $k = 1, 2, \dots$ is the iteration number and where the initial guess $u_2^0(0, t)$ is given.

This corresponds to the so-called "multiplicative" form of the Schwarz algorithm. If we replace the interface condition $\mathcal{G}_2 u_2^k = \mathcal{G}_1 u_1^k$ on Ω_2 by $\mathcal{G}_2 u_2^k = \mathcal{G}_1 u_1^{k-1}$, then we obtain the "additive" version of the algorithm. The multiplicative form converges more rapidly than the additive one but prevents from solving subproblems in parallel (this problem can be circumvented when we are considering more than two subdomains). Note that the study presented in this paper uses the multiplicative form of the algorithm but the results would be exactly the same for the additive form. The usual algorithmic approach applied to ocean-atmosphere climate model generally corresponds to one iteration of the algorithm (2.4) without reaching the convergence, see [4].

A key point for an efficient coupling is to define a good consistency criterion on

the interface Γ by the mean of operators \mathcal{F}_j and \mathcal{G}_j ($j = 1, 2$). In our context we will require the equality of the subproblems solutions and of their fluxes on the interface. The most natural choice to obtain such a connection consists in choosing

$$\mathcal{F}_1 = D_1(0) \frac{\partial}{\partial x} \quad \mathcal{F}_2 = D_2(0) \frac{\partial}{\partial x} \quad \mathcal{G}_1 = \mathcal{G}_2 = Id \quad (2.5)$$

However as proposed in [18], in order to optimize the convergence speed, we can use mixed boundary conditions of Robin type

$$\mathcal{F}_j = D_j(0) \frac{\partial}{\partial x} + \Lambda_1 \quad \mathcal{G}_j = D_j(0) \frac{\partial}{\partial x} + \Lambda_2 \quad (j = 1, 2) \quad (2.6)$$

This type of condition has the advantage to add operators, Λ_1 and Λ_2 , in our coupled problem, which can greatly improve the convergence speed if correctly chosen, as we will see later. In this paper we will focus our attention on *Robin-Robin* type of transmission conditions since *Dirichlet-Neumann* type algorithms are known to converge slowly, except for large discontinuities between the coefficients D_2 and D_1 (they are fully described for example in [22]).

We have now formulated the coupling problem that we want to address. As mentioned previously, the convergence properties of this kind of problem have been extensively studied in the case of constant and continuous diffusion coefficients [10], and there exists also a few results in the case of constant and discontinuous coefficients [13] in the more general case of advection-diffusion-reaction equations.

In this first paper we propose to investigate the problem with diffusion coefficients which are constant on each subdomain and discontinuous at the interface, i.e. $D_j(x) = D_j$, with $D_j > 0$ and $D_1 \neq D_2$. In this case we will be able to prove the convergence of algorithm (2.4) and to determine optimal choices for the Λ_j operators, under some constraints on the parameters of the problem.

2.2 Convergence of the algorithm

A classical approach to demonstrate the convergence of the algorithm is to introduce the error e_j^k between the exact solution u^* and the iterates u_j^k , $j = 1, 2$. If we consider our model problem (2.4) with constant coefficients, by linearity the system satisfied by e_1^k and e_2^k is a homogeneous diffusion equation with homogeneous initial condition :

$$\left\{ \begin{array}{ll} \frac{\partial e_1^k}{\partial t} - \frac{\partial}{\partial x} \left(D_1 \frac{\partial e_1^k}{\partial x} \right) = 0 & \text{in } \Omega_1 \times [0, T] \\ e_1^k(x, 0) = 0 & x \in \Omega_1 \\ \mathcal{B}_1 e_1^k(-L_1, t) = 0 & t \in [0, T] \\ (D_1 \partial_x + \Lambda_1) e_1^k(0, t) = (D_2 \partial_x + \Lambda_1) e_2^{k-1}(0, t), & \text{in } \Gamma \times [0, T] \end{array} \right.$$

$$\left\{ \begin{array}{ll} \frac{\partial e_2^k}{\partial t} - \frac{\partial}{\partial x} \left(D_2 \frac{\partial e_2^k}{\partial x} \right) = 0 & \text{in } \Omega_2 \times [0, T] \\ e_2^k(x, 0) = 0 & x \in \Omega_2 \\ \mathcal{B}_2 e_2^k(L_2, t) = 0 & t \in [0, T] \\ (D_2 \partial_x + \Lambda_2) e_2^k(0, t) = (D_1 \partial_x + \Lambda_2) e_1^k(0, t), & \text{in } \Gamma \times [0, T] \end{array} \right. \quad (2.7)$$

The following part of our analysis is based on a Fourier transform in time denoted for any $g \in L^2(R)$ by $\widehat{g} = \mathcal{F}(g)$, by considering $T \rightarrow \infty$. Note that in our study all the functions are chosen equal to zero for negative time. By a Fourier transform in time the partial differential equations (2.7) reduce to the following ordinary differential equations

$$i\omega \widehat{e}_j^k - D_j \frac{\partial^2 \widehat{e}_j^k}{\partial x^2} = 0 \quad j = 1, 2 \quad (2.8)$$

For $\omega \in R^*$ the characteristic roots are

$$\sigma_j^+ = \sqrt{\frac{i\omega}{D_j}} = \sqrt{\frac{|\omega|}{2D_j}} (1 + \frac{|\omega|}{\omega} i) \quad \text{and} \quad \sigma_j^- = -\sigma_j^+ \quad (2.9)$$

By assuming that the subdomains Ω_1 and Ω_2 are unbounded and that e_j tends to zero for $x \rightarrow \infty$ we find that

$$\widehat{e}_1(x, \omega) = \alpha(\omega) e^{\sigma_1^+ x} \quad \widehat{e}_2(x, \omega) = \beta(\omega) e^{\sigma_2^- x} \quad (2.10)$$

This assumption is usually carried out to simplify the resulting convergence factor and its validity will be discussed in section 5 of this report. Note that the particular case $\omega = 0$ would correspond to the existence of a stationary part in the error. However, since the error is initially zero, such a stationary part is also necessarily zero.

The functions $\alpha(\omega)$ and $\beta(\omega)$ are determined using Robin interface conditions at $x = 0$. If we define λ_j as the *symbol* of operators Λ_j ($j = 1, 2$), i.e.

$$\forall g \in L^2(R) \quad \widehat{\Lambda_j g}(\omega) = \lambda_j(\omega) \widehat{g}(\omega) \quad \forall \omega \in R^* \quad (2.11)$$

α and β at iteration k satisfy the equalities

$$\begin{cases} (D_1 \sigma_1^+ + \lambda_1) \alpha^k(\omega) &= (D_2 \sigma_2^- + \lambda_1) \beta^{k-1}(\omega) \\ (-D_2 \sigma_2^- + \lambda_2) \beta^k(\omega) &= (-D_1 \sigma_1^+ + \lambda_2) \alpha^k(\omega) \end{cases} \quad (2.12)$$

We can define a convergence factor ρ of the Schwarz algorithm by

$$\rho(\omega) = \left| \frac{\widehat{e}_1^k(0, \omega)}{\widehat{e}_1^{k-1}(0, \omega)} \right| = \left| \frac{\widehat{e}_2^k(0, \omega)}{\widehat{e}_2^{k-1}(0, \omega)} \right| \quad (2.13)$$

Therefore, given (2.10), $\rho(\omega) = \left| \frac{\alpha^k(\omega)}{\alpha^{k-1}(\omega)} \right| = \left| \frac{\beta^k(\omega)}{\beta^{k-1}(\omega)} \right|$. Using (2.12) we obtain

$$\rho(\omega) = \left| \frac{(\lambda_1(\omega) + D_2 \sigma_2^-) (\lambda_2(\omega) - D_1 \sigma_1^+)}{(\lambda_1(\omega) + D_1 \sigma_1^+) (\lambda_2(\omega) - D_2 \sigma_2^-)} \right| \quad (2.14)$$

At this point, we are not able to conclude on the convergence (or the divergence) of our algorithm because the operators Λ_j have not been explicitly determined. As we will see in the next section, this is often a difficult task to choose them in an appropriate way. The main difficulty comes from the fact that the convergence factor is formulated in the Fourier space, which leads to act on symbols λ_j but not directly on pseudo-differential operators Λ_j in the physical space.

2.3 Optimized Schwarz Method

The question we intend to adress in this section is: how to choose the transmission conditions in order to obtain the quickest possible convergence ? According to (2.14) we can easily see that the most effective symbols are those which cancel the convergence factor. Therefore they ensure a convergence in only two iterations. Their expressions read

$$\lambda_1^{\text{opt}} = -D_2\sigma_2^- = \sqrt{\frac{|\omega|D_2}{2}}\left(1 + \frac{|\omega|}{\omega}i\right) \quad \lambda_2^{\text{opt}} = D_1\sigma_1^+ = \sqrt{\frac{|\omega|D_1}{2}}\left(1 + \frac{|\omega|}{\omega}i\right) \quad (2.15)$$

These symbols correspond to so-called *absorbing conditions*. Unfortunately, since these optimal symbols are not polynomials in $i\omega$, the absorbing conditions are non local in time in the physical space. Indeed

$$\Lambda_j u_j(x, t) = \mathcal{F}^{-1}(\lambda_j) * u_j(x, t) = \int_{-\infty}^{+\infty} \mathcal{F}^{-1}(\lambda_j)(\tau) u_j(x, t - \tau) d\tau \quad (2.16)$$

As a consequence, the new problem now is to find local operators which are a good approximation of nonlocal ones. By noting that

$$\forall f \in C^m \cap L^1(R), k \in \llbracket 1, n \rrbracket \quad \widehat{f^{(k)}}(\xi) = (i\omega)^k \widehat{f}(\xi) \quad (2.17)$$

the aim is thus to find a polynomial form in $i\omega$ which is a good approximation of λ_j^{opt} .

There are mainly two approaches for such an approximation. The first one consists in a low frequency approximation, namely a Taylor expansion for a small ω , but this methodology is unrelavant in our study because we want to be able to consider a wide range of frequencies. The second and more sophisticated approach is to solve a minimax problem in order to determine local operators that optimize the convergence speed over the full range of frequencies $[\omega_{\min}, \omega_{\max}]$. For a zeroth order approximation we look for parameters $p_j \in R$ such that $\lambda_j^{\text{opt}} \approx p_j$, which are solutions of the optimization problem

$$\min_{p_1, p_2 \in R} \left(\max_{\omega \in [\omega_{\min}, \omega_{\max}]} \rho(p_1, p_2, \omega, D_1, D_2) \right) \quad (2.18)$$

Because in practice we are working on a discrete problem the frequencies allowed by our temporal grid range from $\omega_{\min} = \frac{\pi}{T}$ to $\omega_{\max} = \frac{\pi}{\Delta t}$ where Δt is the time step.

Similarly, looking for a first order approximation would consist in making the approximation $\lambda_j^{\text{opt}} \approx p_j + i\omega q_j$, and solving $\min_{p_j, q_j \in R} \left(\max_{\omega \in [\omega_{\min}, \omega_{\max}]} \rho(p_1, p_2, q_1, q_2, \omega, D_1, D_2) \right)$.

The analytical resolution of problem (2.18) is not an easy task: indeed the minimisation of a maximum is known to be one of the most difficult problem in optimization theory. On top of that, we are working on an optimization for two parameters p_1 and p_2 (4 parameters for the first order approximation) which strengthen the difficulty. Some analytical results exist in the case of *two-sided* optimisation for 2D steady-state diffusion equation in [19] and [5], and for 2D Helmholtz equation in [12]. In [13], in the case of an advection-diffusion-reaction problem, the asymptotic solution of (2.18) for $\Delta t \rightarrow 0$ and for a positive advection is found in two particular cases: first $p_1 = p_2$, and second $p_1 \neq p_2$ but

$D_1 = D_2$. In this paper we intend to study (2.18) in a general case $p_1 \neq p_2$ and $D_1 \neq D_2$.

Solving numerically the previous minimax problems is quite expensive from a computational point of view, and this optimization must be performed for any change in the values of D_1 and D_2 . That is why we intend in the following to find an analytical solution in the case of a zeroth order approximation. This will be done with two different sets of interface conditions, namely *Neumann-Robin* and *Robin-Robin*.

Part II

The constant coefficients case

3 Optimized Schwarz method with *Neumann-Robin* interface conditions

It sometimes happens that one of the two subdomains corresponds to a model seen as a "blackbox", which inputs and outputs are fluxes (i.e. Neumann conditions). This may be the case for example when one has to couple his own model with an "external" model the source code of which he cannot access or he does not want to modify.

In this section, we will assume that the solution in Ω_2 is subject to a Neumann boundary condition. This relatively easy case is also treated separately because it introduces several basic ideas of the more general Robin-Robin interface conditions.

Imposing a Neumann boundary condition for the solution u_2 on Γ corresponds to the choice of $\Lambda_2 = 0$ in the previous general formulation. The convergence factor ρ_{NR} (NR stands for "Neumann-Robin"), obtained from (2.14), reduces to

$$\rho_{\text{NR}} = \left| \frac{D_1 \sigma_1^+ (D_2 \sigma_2^- + \lambda_1)}{D_2 \sigma_2^- (D_1 \sigma_1^+ + \lambda_1)} \right| \quad (3.1)$$

Introducing $\zeta = \sqrt{|\omega| D_1}$, $\gamma = \sqrt{\frac{D_2}{D_1}}$, $\lambda_1 = \frac{\sqrt{\zeta_{\min} \zeta_{\max}}}{2} p$ ($p \in \mathbb{R}$), and using the expression (2.9) for σ_1^+ and σ_2^- , we obtain

$$\rho_{\text{NR}}(p, \zeta) = \frac{1}{\gamma} \sqrt{\frac{(p - \gamma \zeta)^2 + \gamma^2 \zeta^2}{(p + \zeta)^2 + \zeta^2}} \quad (3.2)$$

with $\zeta = \zeta / \sqrt{\zeta_{\max} \zeta_{\min}}$.

It can easily be shown that for $p > 0$, $\gamma > 0$ and $\zeta > 0$ we have $\rho_{\text{NR}}(p, \zeta) < \rho_{\text{NR}}(-p, \zeta)$.

We can thus assume that p is strictly positive for our study. We define an additional parameter $\mu = \sqrt{\zeta_{\max} / \zeta_{\min}}$, we thus get that ζ varies between $\zeta_{\min} = \mu^{-1}$ and $\zeta_{\max} = \mu$.

We now aim at optimizing the convergence speed, by finding p^* the solution of the minimax problem:

$$\min_{p > 0} \left(\max_{\zeta \in [\mu^{-1}, \mu]} \rho_{\text{NR}}(p, \zeta) \right). \quad (3.3)$$

Theorem 3.1 (Optimized Robin parameter) *The analytical solution of the minimax problem (3.3) is given by*

$$p^* = \frac{1}{2} \left(-v^* + \sqrt{8\gamma + (v^*)^2} \right) \quad (3.4)$$

where

$$v^* = (1 - \gamma)\beta, \text{ with } \beta = \mu + 1/\mu$$

Proof: first we study the behaviour of the derivative of ρ_{NR} with respect to ζ and p (with $\zeta \geq 0$ and $p \geq 0$). We define the variable q by $q = p / \left(\gamma - 1 + \sqrt{1 + \gamma^2} \right)$. q will not be used in the computations but simplifies the proof of the two followings properties: restriction of the parameter range and equioscillation property.

Restriction of the parameters range

We get that

$$\text{Sign} \left(\frac{\partial \rho_{\text{NR}}}{\partial p} \right) = \text{Sign} (q - \zeta) \quad (3.5)$$

Looking at the sign of the derivative of ρ_{NR} with respect to p , it appears that, for all values of ζ , ρ_{NR} is a decreasing function of p for $q < \zeta_{\text{min}} = \mu^{-1}$. This proves that $q^* \geq \zeta_{\text{min}}$. A similar argument shows that $q^* \leq \zeta_{\text{max}}$. This shows that the optimized parameter q^* must satisfy

$$1/\mu \leq q^* \leq \mu \quad (3.6)$$

Along with (3.5), this shows that the convergence factor has to be a decreasing function of p at $\zeta = 1/\mu$ and an increasing function of p at $\zeta = \mu$.

Equioscillation property

Let's have a look at the derivative of ρ_{NR} with respect to ζ .

$$\text{Sign} \left(\frac{\partial \rho_{\text{NR}}}{\partial \zeta} \right) = \text{Sign} (\zeta - q) \quad (3.7)$$

This relation implies that ρ_{NR} has a local minima between μ^{-1} and μ . The maximum value of the convergence factor is thus attained either at $\zeta = 1/\mu$ or at $\zeta = \mu$ (or both). If we assume $\rho_{\text{NR}}(p, \mu^{-1}) < \rho_{\text{NR}}(p, \mu)$ it is always possible to decrease the maximum value of $\rho_{\text{NR}}(p, \zeta)$ by decreasing the value of p so that we must have $\rho_{\text{NR}}(p, 1/\mu) \geq \rho_{\text{NR}}(p, \mu)$.

A similar argument shows that $\rho_{\text{NR}}(p, \mu) \geq \rho_{\text{NR}}(p, 1/\mu)$. Thus the optimal parameter must satisfy the equioscillation property $\rho_{\text{NR}}(p^*, 1/\mu) = \rho_{\text{NR}}(p^*, \mu)$.

After simple computations, we find that p^* must be the solution of

$$(\gamma - 1) (\mu + 1/\mu) + \frac{2\gamma}{p^*} - p^* = 0$$

If we introduce $v^* = \frac{2\gamma}{p^*} - p^*$, $v^* = (1 - \gamma) (\mu + 1/\mu)$ and the unique positive solution of the equation $v^* = \frac{2\gamma}{p^*} - p^*$ is given by $p^* = \frac{1}{2} \left(-v^* + \sqrt{8\gamma + (v^*)^2} \right)$.

■

We found that the convergence factor satisfies an equioscillation property. This concept of equioscillation property comes from the Chebyshev's alternant theorem (or equioscillation theorem). This theorem states that for a given continuous function u on $[a, b]$, $P_u(x)$ is the best polynomial approximation of u in $\mathcal{P}_N[X]$ in the sense of the L^∞ -norm if and only if we can find $N + 2$ points x_j in $[a, b]$ such that $|u - P_u|$ is maximum for each x_j , i.e. $\forall j, |u(x_j) - P_u(x_j)| = \max_{x \in [a, b]} |u - P_u|$.

The similarities between the Chebyshev's theorem and Optimized Schwarz Method are clearly exposed in [5] and [2].

A typical optimized convergence factor $\rho_{\text{NR}}(p^*)$ is shown in figure 2 for $\gamma = 5, \mu = 6$.

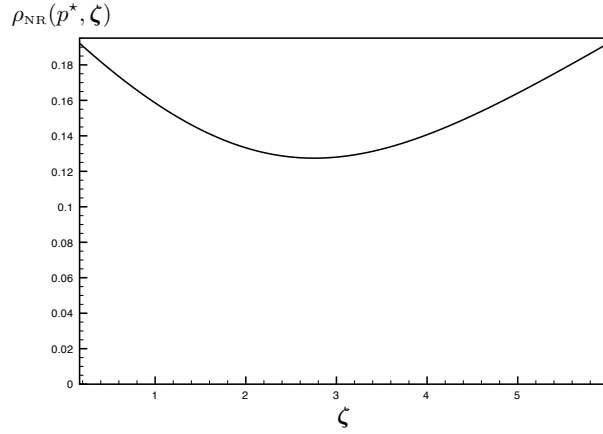


Figure 2: Behaviour of $\rho_{\text{NR}}(p^*, \zeta)$ with respect to ζ , for $\gamma = 5$ and $\mu = 6$.

Figure 3 shows the variation with γ of the convergence factor and the optimal parameter p^* for $\mu = 2$ and $\mu = 6$. Note that the ratio between minimum and maximum frequencies $\frac{\omega_{\text{max}}}{\omega_{\text{min}}}$ is given by $\frac{\omega_{\text{max}}}{\omega_{\text{min}}} = \mu^4$ which equals 16 for $\mu = 2$ and 1296 for $\mu = 6$. We look at three particular cases: $\gamma \rightarrow 0^+, \gamma = 1$ and

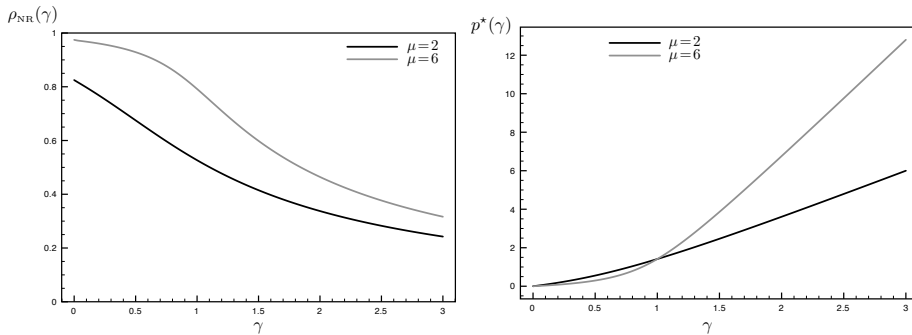


Figure 3: Convergence factor (left) and optimal parameter p^* (right) for $\mu = 2$ and $\mu = 6$ as a function of γ

$\gamma \rightarrow \infty$.

- $\gamma \rightarrow 0^+$ ($D_1 \gg D_2$)

$$\lim_{\gamma \rightarrow 0^+} \rho_{\text{NR}}^* = \sqrt{1 - \frac{2}{\beta^2}}, \quad \lim_{\gamma \rightarrow 0^+} p^* = 0$$

The minimum value of the convergence factor is attained at $\mu = 1$ (i.e. $\beta = 2$) and is equal to $\frac{\sqrt{2}}{2}$. When μ is increased, the convergence is very slow. The optimal boundary condition tends towards a Neumann-Neumann operator.

- $\gamma = 1$ ($D_1 = D_2$)

$$\rho_{\text{NR}}^* = \sqrt{\frac{\beta - \sqrt{2}}{\beta + \sqrt{2}}}, \quad p^* = \sqrt{2}$$

ρ_{NR}^* approaches 1 when μ (or β) is increased.

- $\gamma \rightarrow +\infty$ ($D_1 \ll D_2$)

$$\lim_{\gamma \rightarrow +\infty} \rho_{\text{NR}}^* = 0, \quad \lim_{\gamma \rightarrow +\infty} p^* = +\infty$$

When γ tends to $+\infty$, the convergence is very fast (the convergence factor approaches 0) and the optimal boundary condition tends towards a Neumann-Dirichlet operator. The Dirichlet boundary condition has to be imposed at the boundary of the domain with the smaller diffusion coefficient (Ω_1).

We conclude that zeroth-order optimized Neumann-Robin boundary conditions are only efficient when $D_1 \ll D_2$. In the next section, we study the zeroth-order two-sided Robin-Robin boundary conditions.

4 OSM for a diffusion problem with discontinuous (but constant) coefficients: two-sided Robin transmission conditions

Let's suppose now that we have access to both numerical codes. In this configuration the best strategy is to optimize the conditions on both sides of the interface to obtain a faster convergence speed.

By keeping the notations ζ , ζ , μ and γ defined in the previous section and by approximating λ_1^{opt} and λ_2^{opt} respectively by $\frac{\sqrt{\zeta_{\min}\zeta_{\max}}}{2} p_2$ and $\frac{\sqrt{\zeta_{\min}\zeta_{\max}}}{2} p_1$ the convergence factor ρ_{RR} reads

$$\rho_{\text{RR}}(p_1, p_2, \zeta) = \sqrt{\frac{((p_1 - \zeta)^2 + \zeta^2) ((p_2 - \gamma\zeta)^2 + \gamma^2\zeta^2)}{((p_1 + \gamma\zeta)^2 + \gamma^2\zeta^2) ((p_2 + \zeta)^2 + \zeta^2)}} \quad (4.8)$$

We can easily demonstrate that, for nonnegative fixed values of ζ and γ and for $p_1, p_2 > 0$ we have $\rho_{\text{RR}}(p_1, p_2, \zeta) < \rho_{\text{RR}}(-p_1, -p_2, \zeta)$, as well as $\rho_{\text{RR}}(p_1, p_2, \zeta) < \rho_{\text{RR}}(p_1, -p_2, \zeta)$ and $\rho_{\text{RR}}(p_1, p_2, \zeta) < \rho_{\text{RR}}(-p_1, p_2, \zeta)$. Those three inequalities show that we can restrict our study to strictly positive values of p_1 and p_2 (note that $p_1 = 0$ or $p_2 = 0$ corresponds to the *Neumann-Robin* case studied previously, and that $p_1 = p_2 = 0$ leads to a *Neumann-Neumann* type algorithm).

In the following, we will suppose that $\gamma \geq 1$. The problem being now symmetric, optimal parameters p_1 and p_2 for the case $\gamma \leq 1$ can be obtained by interverting optimal values for the case $\gamma \geq 1$.

The next step is now to tune the values of the free parameters p_1 and p_2 to improve the convergence properties. As mentioned previously the most powerful way to do this is to solve the following optimisation problem

$$\min_{p_1, p_2 > 0} \left(\max_{\zeta \in [\mu^{-1}, \mu]} \rho_{\text{RR}}(p_1, p_2, \zeta) \right) \quad (4.9)$$

4.1 Behaviour of the convergence factor with respect to the Robin parameters

First, we propose to study the behaviour of ρ_{RR} with respect to the parameters p_1 and p_2 . Let us introduce two new parameters q_1 and q_2 defined by

$$q_1 = \frac{p_1}{1 - \gamma + \sqrt{1 + \gamma^2}} \quad q_2 = \frac{p_2}{\gamma - 1 + \sqrt{1 + \gamma^2}} \quad (4.10)$$

We first remark that for $\gamma \geq 1$ and $q_1 \leq q_2$, we have $\rho_{\text{RR}}(p_1, p_2, \zeta) \leq \rho_{\text{RR}}(p_2, p_1, \zeta)$. This proves that the optimal parameters satisfy $q_1^* \leq q_2^*$. This implies that $p_1 \leq p_2$ and that $p_1 < p_2$ if $\gamma > 1$. This immediately proves that *one-sided* ($p_1 = p_2$) Robin-Robin boundary conditions are not optimal as soon as $\gamma > 1$.

Restriction of the parameters range

It can easily be shown that $\text{Sign} \left(\frac{\partial \rho_{\text{RR}}}{\partial p_1} \right) = \text{Sign}(q_1 - \zeta)$ and $\text{Sign} \left(\frac{\partial \rho_{\text{RR}}}{\partial p_2} \right) = \text{Sign}(q_2 - \zeta)$. This implies that

$$\begin{aligned} \frac{\partial \rho_{\text{RR}}}{\partial p_1} > 0 \text{ when } \zeta < q_1 & \quad \frac{\partial \rho_{\text{RR}}}{\partial p_1} < 0 \text{ when } \zeta > q_1 \\ \frac{\partial \rho_{\text{RR}}}{\partial p_2} > 0 \text{ when } \zeta < q_2 & \quad \frac{\partial \rho_{\text{RR}}}{\partial p_2} < 0 \text{ when } \zeta > q_2 \end{aligned} \quad (4.11)$$

Looking at the sign of the derivatives of ρ_{RR} with respect to p_1 and p_2 , it appears that if we choose $q_1 < \zeta_{\text{min}} = \mu^{-1}$, we can decrease the convergence factor by increasing p_1 , indeed $\frac{\partial \rho_{\text{RR}}}{\partial p_1} < 0, \forall q_1 > \zeta_{\text{min}}$. A similar argument shows that $q_2 \leq \zeta_{\text{max}}$. This shows that the optimized parameters q_1^* and q_2^* must satisfy

$$\mu^{-1} \leq q_1^* < q_2^* \leq \mu \quad (4.12)$$

(4.11) and (4.12) imply that at $\zeta = 1/\mu$, ρ_{RR} is an increasing function of p_1 and p_2 (or q_1 and q_2) while at $\zeta = \mu$, ρ_{RR} is an decreasing function of p_1 and p_2 (or q_1 and q_2).

4.2 Extrema of ρ_{RR} with respect to ζ

The next step to solve (4.9) analytically is to find the location of the extrema of $\rho_{RR}(p_1, p_2, \zeta, \gamma)$ with respect to ζ .

Theorem 4.1 (Extrema of $\rho_{RR}(\zeta)$) $\rho_{RR}(p_1, p_2, \zeta)$ has one or three positive local extrema. In the case of one extremum, it corresponds to a minimum and is located at $\chi = \sqrt{\frac{p_1 p_2}{2\gamma}}$.

Proof: We start by the following property that can easily be verified:

$$\rho_{RR}(p_1, p_2, \zeta) = \rho_{RR}(p_1, p_2, \chi^2/\zeta), \text{ where } \chi = \sqrt{\frac{p_1 p_2}{2\gamma}}$$

After derivation with respect to ζ , this leads to

$$\frac{\partial \rho_{RR}}{\partial \zeta}(p_1, p_2, \zeta) = -\frac{\chi^2}{\zeta^2} \frac{\partial \rho_{RR}}{\partial \zeta}(p_1, p_2, \chi^2/\zeta) \quad (4.13)$$

which shows that $\frac{\partial \rho_{RR}}{\partial \zeta}(p_1, p_2, \pm\chi) = 0$.

$\frac{\partial \rho_{RR}}{\partial \zeta}(p_1, p_2, \zeta)$ has the sign of $P(\zeta)$ a (unitary) sixth order polynomial. Thus $P(\zeta)$ has either two or six real roots, two of them being given by $\zeta = \pm\chi$.

Let's suppose that $P(\zeta)$ has six real roots. We are going to show that only three of these six roots (including $\zeta = \chi$) are positive. From (4.13) we see that if ζ^0 is a root of $P(\zeta)$, $\zeta^1 = \chi^2/\zeta^0$ is a root too.

Let's suppose that the four other roots are positive. Then we have

$$\zeta_5 = -\chi \leq 0 \leq \zeta_6 \leq \zeta_1 \leq \zeta_2 = \chi \leq \zeta_3 (= \frac{\chi^2}{\zeta_1}) \leq \zeta_4 (= \frac{\chi^2}{\zeta_6})$$

and the sum of the six roots must be greater than 2χ . However the sum of the six roots of $P(\zeta)$ is given by $-a_5$ where a_5 is the coefficient of the ζ^5 term and is equal to $a_5 = \frac{(\gamma-1)(p_2-p_1)}{\gamma}$. Using the fact that $\gamma \geq 1$ and that (4.12) implies $p_2 \geq p_1$, $-a_5$ cannot be positive so that we conclude that we have at most three positive roots of $P(\zeta)$.

It can be verified that $P(0) < 0$ and $P(+\infty) > 0$ so that if only one positive root exist (at $\zeta = \chi$), it is a local minimum. ■

4.3 Equioscillation of ρ_{RR} at the end points

Theorem 4.2 (Equioscillation at the end points) The optimized convergence factor $\rho_{RR}(p_1^*, p_2^*, \zeta)$ satisfies

- $\rho_{RR}(p_1^*, p_2^*, \chi) \leq \max(\rho_{RR}(p_1^*, p_2^*, \mu^{-1}), \rho_{RR}(p_1^*, p_2^*, \mu))$
- the equioscillation property:
 $\rho_{RR}(p_1^*, p_2^*, \mu^{-1}) = \rho_{RR}(p_1^*, p_2^*, \mu)$ which holds only for $p_1^* p_2^* = 2\gamma$

Proof: We first demonstrate that $\rho_{\text{RR}}(p_1^*, p_2^*, \chi) \leq \max(\rho_{\text{RR}}(p_1^*, p_2^*, \mu^{-1}), \rho_{\text{RR}}(p_1^*, p_2^*, \mu))$.

If χ is the only positive root of $\frac{\partial \rho_{\text{RR}}(\zeta)}{\partial \zeta}$, this is trivial since χ is a local minimum.

Let's look at the case where there are three positive roots, in this case χ is a local maximum.

From the identity $\chi = \sqrt{\frac{p_1 p_2}{2\gamma}} = \sqrt{q_1 q_2}$ and (4.12) $1/\mu \leq q_1 \leq q_2 \leq \mu$ we get

$$1/\mu \leq q_1 \leq \chi = \sqrt{q_1 q_2} \leq q_2 \leq \mu \quad (4.14)$$

We already know that at $\zeta = 1/\mu$, ρ_{RR} is a decreasing function of q_1 and that at $\zeta = \mu$, ρ_{RR} is an increasing function of q_1 . (4.14) shows that at $\zeta = \chi$, ρ_{RR} is an increasing function of q_1 since $q_1 \leq \chi$. If we suppose that $\rho_{\text{RR}}(p_1^*, p_2^*, \chi) \geq \rho_{\text{RR}}(p_1^*, p_2^*, \mu^{-1})$ then we always can decrease q_1 (or p_1) such that it improves the convergence factor (by reducing the values both at $\zeta = \chi$ and at $\zeta = \mu$). Playing with q_2 we can similarly prove that $\rho_{\text{RR}}(p_1^*, p_2^*, \chi) \leq \rho_{\text{RR}}(p_1^*, p_2^*, \mu)$.

Note that this also demonstrates that $\zeta_1 \geq 1/\mu$ and $\zeta_3 \leq \mu$.

This is sufficient to fully describe the behaviour of the convergence factor with respect to q_1 , q_2 and ζ , as shown in figure 4. In practice, the two cases will be differentiated by the sign of the second order derivate of $\rho_{\text{RR}}(p_1, p_2, \zeta)$ at $\zeta = \chi$.

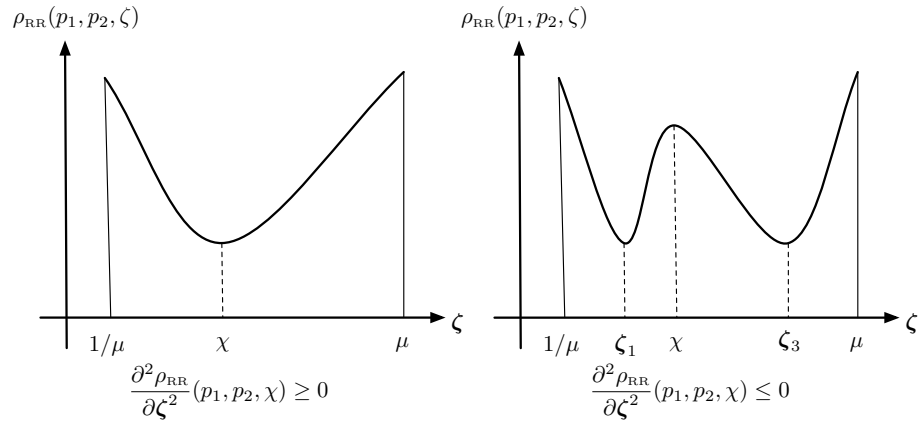


Figure 4: Behaviour of the convergence factor with respect to ζ

The following proves that the values taken by $\rho_{\text{RR}}(p_1^*, p_2^*, \zeta)$ at the two end points $\zeta = 1/\mu$, $\zeta = \mu$ are equal.

Indeed if we consider $\rho_{\text{RR}}(p_1, p_2, 1/\mu) < \rho_{\text{RR}}(p_1, p_2, \mu)$ (resp. $\rho_{\text{RR}}(p_1, p_2, 1/\mu) > \rho_{\text{RR}}(p_1, p_2, \mu)$), it is always possible to decrease the maximum value of $\rho_{\text{RR}}(\zeta)$ by increasing (resp. decreasing) the values of p_1 (resp. p_2). Thus the optimal parameters must satisfy $\rho_{\text{RR}}(p_1^*, p_2^*, \mu^{-1}) = \rho_{\text{RR}}(p_1^*, p_2^*, \mu)$: the equioscillation property.

This holds for

$$(p_1 + p_2)(2\gamma - p_1 p_2)S(p_1, p_2, \mu, \gamma) = 0 \quad (4.15)$$

with

$$\begin{aligned} S(p_1, p_2, \mu, \gamma) &= 2[(1 + \gamma^2) - \gamma(\mu + \mu^{-1})^2] p_1 p_2 + (\gamma - 1)(\mu + 1/\mu)(p_1 - p_2)(2\gamma + p_1 p_2) \\ &+ 2\gamma(p_1 - p_2)^2 - (2\gamma - p_1 p_2)^2 \end{aligned} \quad (4.16)$$

Obviously all couple p_1, p_2 that satisfies the relation $p_1 p_2 = 2\gamma$ are solutions to (4.15). We are now going to show that there are no other admissible values. Other potential solutions of the problem are the solutions of $S(p_1, p_2, \mu) = 0$. S can be seen as a second order polynomial in p_2 and thus have two real solutions:

$$p_2 = f_1(p_1) \quad p_2 = f_2(p_1) \quad (4.17)$$

If we assume that p_2 is related to p_1 with one of the relations (4.17), looking at the figure 4 we can argue that for any couple (p_1, p_2) we must have $dp_2/dp_1 < 0$ to satisfy an equioscillation property. Indeed let $\rho_{\text{RR}}^\dagger(p_1, \zeta)$ be defined by

$$\rho_{\text{RR}}^\dagger(p_1, \zeta) = \rho_{\text{RR}}(p_1, p_2(p_1), \zeta)$$

Then

$$\frac{\partial \rho_{\text{RR}}^\dagger(p_1, \zeta)}{\partial p_1} = \frac{\partial \rho_{\text{RR}}(p_1, p_2(p_1), \zeta)}{\partial p_1} + \frac{\partial \rho_{\text{RR}}(p_1, p_2(p_1), \zeta)}{\partial p_2} \frac{dp_2}{dp_1} \quad (4.18)$$

We have already proved that the following properties must hold

$$\begin{aligned} \frac{\partial \rho_{\text{RR}}(p_1, p_2(p_1), 1/\mu)}{\partial p_1} &> 0, \quad \frac{\partial \rho_{\text{RR}}(p_1, p_2(p_1), 1/\mu)}{\partial p_2} > 0 \\ \frac{\partial \rho_{\text{RR}}(p_1, p_2(p_1), \mu)}{\partial p_1} &< 0, \quad \frac{\partial \rho_{\text{RR}}(p_1, p_2(p_1), \mu)}{\partial p_2} < 0 \end{aligned} \quad (4.19)$$

If we suppose $dp_2/dp_1 > 0$ then (4.18) and (4.19) show that $\rho_{\text{RR}}^\dagger(p_1, 1/\mu)$ is an increasing function of p_1 while $\rho_{\text{RR}}^\dagger(p_1, \mu)$ is a decreasing function of p_1 , thus (4.19) and the equioscillation property cannot be satisfied at the same time if $dp_2/dp_1 > 0$.

It can be shown that the two solutions given by (4.17) do not verify this last condition. Indeed one can prove that we have $df_1/dp_1 > 0$ and $df_2/dp_1 > 0$. Details of the computations are omitted here but we mention that the only conditions necessary to find this result are $\gamma > 0, \mu > 1$.

We can conclude that $p_1 p_2 = 2\gamma$ is the only solution which leads to an equioscillation property. ■

Let us mentioned that this implies that $\chi = \sqrt{\frac{p_1 p_2}{2\gamma}} = 1$ and that

$$\rho_{\text{RR}}(p_1^*, p_2^*, \zeta) = \rho_{\text{RR}}(p_1^*, p_2^*, 1/\zeta) \quad \forall \zeta \in [1/\mu, \mu]$$

4.4 Solution of the minmax problem

The convergence factor is now a function of p_1 and ζ only:

$$\rho_{\text{RR}}^\dagger(p_1, \zeta) = \rho_{\text{RR}}(p_1, 2\gamma/p_1, \zeta)$$

Lemma 4.1 *The solution of the minmax problem is given by the solution of the minimization of $\rho_{RR}^\dagger(p_1, 1/\mu)$. The minimization must be done under the constraint that $p_1^* \geq p_1^{*,\text{equi}}$ where $p_1^{*,\text{equi}}$ is the solution of the three points equioscillation problem $\rho_{RR}^\dagger(p_1, 1) = \rho_{RR}^\dagger(p_1, 1/\mu) = \rho_{RR}^\dagger(p_1, \mu)$*

Figure 4 ables us to remark that the resolution of the minmax problem corresponds to the minimization of $\rho_{RR}^\dagger(p_1, 1/\mu)$ (or $\rho_{RR}^\dagger(p_1, \mu)$) with respect to p_1 . If we are in the case where $\chi = 1$ is a local maximum, the additional constraint given by theorem (4.2) must be imposed

$$\rho_{RR}^\dagger(p_1, 1) \leq \rho_{RR}^\dagger(p_1, 1/\mu) \quad (4.20)$$

Knowing that $p_1 p_2 = 2\gamma$ or equivalently $q_1 q_2 = 1$, the range of admissible values given by (4.12) can now be written $1/\mu \leq q_1 \leq 1$ and translates in terms of the variable p_1 :

$$p_1 \in [p_{1,\min}, p_{1,\max}] \text{ where } p_{1,\min} = (1 - \gamma + \sqrt{1 + \gamma^2})/\mu, \quad p_{1,\max} = (1 - \gamma + \sqrt{1 + \gamma^2}) \quad (4.21)$$

Moreover it can be shown that $\rho_{RR}^\dagger(p_1, 1)$ is a decreasing function of p_1 . So that the constraint (4.20) can also be written $p_1^* \geq p_1^{*,\text{equi}}$ where $p_1^{*,\text{equi}}$ is the solution of a three points equioscillation problem $\rho_{RR}^\dagger(p_1^{*,\text{equi}}, 1) = \rho_{RR}^\dagger(p_1^{*,\text{equi}}, 1/\mu) = \rho_{RR}^\dagger(p_1^{*,\text{equi}}, \mu)$.

We are now looking at the minimization of $\rho_{RR}^\dagger(p_1, 1/\mu)$ for $p_1 \in [p_{1,\min}, p_{1,\max}]$.

Lemma 4.2 *For $\gamma > 1$, the derivative of $\rho_{RR}^\dagger(p_1, 1/\mu)$ has exactly one root in the range $[p_{1,\min}, p_{1,\max}]$. This root corresponds to a local minimum of $\rho_{RR}^\dagger(p_1, 1/\mu)$. In the special case $\gamma = 1$, $p_1 = p_{1,\max} (= \sqrt{2})$ is always a root of $\frac{\partial \rho_{RR}^\dagger}{\partial p_1}(p_1, 1/\mu)$.*

The derivative of $\rho_{RR}^\dagger(p_1, 1/\mu)$ can be written under the following form:

$$\frac{\partial \rho_{RR}^\dagger}{\partial p_1}(p_1, 1/\mu) = g(p_1, \mu)N(p_1, \mu)$$

where g is a strictly positive function and $N(p_1, \mu)$ a six order polynomial in p_1 . The change of variable $v = 2\gamma/p_1 - p_1$ transforms $N(p_1, \mu)$ in

$$N(p_1, \mu) = p_1^3 Q(v)$$

where $Q(v)$ is the third order polynomial given by

$$Q(v) = 8(\gamma - 1)(1 + \gamma^2) + 2\beta(\gamma\beta^2 - 3(1 + \gamma^2))v + 2(\gamma - 1)\beta^2 v^2 - \beta v^3 \quad (4.22)$$

where $\beta = 1/\mu + \mu$.

It can be shown that, for $\gamma > 1$, this polynomial has only one root in $[v_{\min}, v_{\max}]$ where, according to (4.21), v_{\min} and v_{\max} are given by

$$v_{\min} = 2(\gamma - 1), \quad v_{\max} = (\gamma - 1)\beta + \sqrt{1 + \gamma^2}\sqrt{\beta^2 - 4} \quad (4.23)$$

This root corresponds to a minimum of $\rho_{\text{RR}}^\dagger(p_1, 1/\mu)$ since it can be found that $\frac{\partial \rho_{\text{RR}}^\dagger}{\partial p_1}(p_{1,\min}, 1/\mu) \leq 0$ and $\frac{\partial \rho_{\text{RR}}^\dagger}{\partial p_1}(p_{1,\max}, 1/\mu) \geq 0$.

For $\gamma = 1$, $v = v_{\min} = 0$ (i.e. $p_1 = p_{1,\max} = \sqrt{2}$) is always a root of $Q(v)$.

Figure (5) exhibits the variations of $\rho_{\text{RR}}^\dagger(p_1, 1/\mu)$ with p_1 . p_1^{\min} is the location of the minimum of $\rho_{\text{RR}}^\dagger(p_1, 1/\mu)$ over $[p_{1,\min}, p_{1,\max}]$.

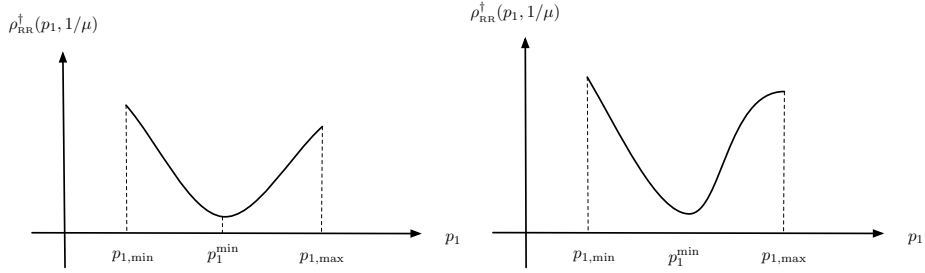


Figure 5: Behaviour of $\rho_{\text{RR}}^\dagger(p_1, 1/\mu)$ with respect to p_1 . The general case ($\gamma > 1$) is on the left and the special case $\gamma = 1$ on the right

The solution of the constrained minimization problem is now easily handled: if $p_1^{\min} \leq p_1^{*,\text{equi}}$ the solution of the minmax problem is given by $p_1^{*,\text{equi}}$, otherwise the solution of the minmax problem is given by p_1^{\min} .

The inequality $p_1^{\min} \leq p_1^{*,\text{equi}}$ is satisfied if and only if $\frac{\partial \rho_{\text{RR}}^\dagger}{\partial p_1}(p_1^{*,\text{equi}}, \mu) \geq 0$ or equivalently $Q(v^{*,\text{equi}}) \geq 0$ (where $v^{*,\text{equi}} = 2\gamma/p_1^{*,\text{equi}} - p_1^{*,\text{equi}}$).

Finally the following result will be useful: for $v \geq v_{\max}$ or equivalently $p_1 \leq p_{1,\min}$ we have $Q(v) \leq 0$ (or $\frac{\partial \rho_{\text{RR}}^\dagger(p_1, 1/\mu)}{\partial p_1} \leq 0$). Indeed using relation (4.18) at $\zeta = 1/\mu$:

$$\frac{\partial \rho_{\text{RR}}^\dagger(p_1, 1/\mu)}{\partial p_1} = \frac{\partial \rho_{\text{RR}}(p_1, p_2(p_1), 1/\mu)}{\partial p_1} + \frac{\partial \rho_{\text{RR}}(p_1, p_2(p_1), 1/\mu)}{\partial p_2} \frac{dp_2}{dp_1}$$

If $p_1 \leq p_{1,\min}$, $\frac{\partial \rho_{\text{RR}}(p_1, p_2(p_1), 1/\mu)}{\partial p_1} < 0$, but through the relation $p_2 = 2\gamma/p_1$, we have $p_2 \geq p_{2,\max} (= (\gamma - 1 + \sqrt{1 + \gamma^2}) \mu)$ so that $\frac{\partial \rho_{\text{RR}}(p_1, p_2(p_1), 1/\mu)}{\partial p_2} \geq 0$.

Using $\frac{dp_2}{dp_1} = -2\gamma/p_1^2 \leq 0$, this proves that $\frac{\partial \rho_{\text{RR}}^\dagger(p_1, 1/\mu)}{\partial p_1} \leq 0$.

We are now left with the problem of finding the solution of the three point equioscillation problem.

Theorem 4.3 (Equioscillation between 3 points) *The only parameters $p_1^{*,\text{equi}}$ and $p_2^{*,\text{equi}}$, such that $p_1^{*,\text{equi}} \leq p_{1,\max}$, that satisfy an equioscillation of the con-*

vergence factor ρ_{RR} between the three points $(1/\mu, 1, \mu)$ are

$$\begin{cases} p_1^{*,\text{equi}} = \frac{1}{2} \left[-v^{*,\text{equi}} + \sqrt{8\gamma + (v^*)^2} \right] \\ p_2^{*,\text{equi}} = 2\gamma \left(p_1^{*,\text{equi}} \right)^{-1} \end{cases}$$

where

$$v^{*,\text{equi}} = \frac{1}{2} \left[(2 + \beta)(\gamma - 1) + \sqrt{4(1 + \gamma)^2(\beta - 1) + \beta^2(\gamma - 1)^2} \right] \quad (4.24)$$

Proof: We have to find the solution of the problem $\rho_{RR}^\dagger(p_1, 1/\mu) = \rho_{RR}^\dagger(p_1, 1)$. It can be shown that this is equivalent to the search of the zeros of a fourth order polynomial $R(p_1)$ that can be written under the form

$$R(p_1) = p_1^2 T(v), \quad T(v) = 2(1 + \gamma^2) - 4\gamma\beta + (1 - \gamma)(2 + \beta)v + v^2$$

where v is again defined by $v = 2\gamma/p_1 - p_1$.

The unique root of $T(v)$ that satisfies $v \geq v_{\min}$ (i.e. $p_1 \leq p_{1,\max}$) is given by

$$v^{*,\text{equi}} = \frac{1}{2} \left[(2 + \beta)(\gamma - 1) + \sqrt{4(1 + \gamma)^2(\beta - 1) + \beta^2(\gamma - 1)^2} \right]$$

and $p_1^{*,\text{equi}}$ is deduced from the relation between p_1 and v . ■

Putting everything together the solution of the minmax problem is given by

Theorem 4.4 *The optimal parameters of the minmax problem are given by*

$$\begin{cases} p_1^* = \frac{1}{2} \left[-v^* + \sqrt{8\gamma + (v^*)^2} \right] \\ p_2^* = 2\gamma/p_1^* = p_1^* + v^* \end{cases}$$

where

$$v^* = \begin{cases} v^{*,\text{equi}} & \text{if } Q(v^{*,\text{equi}}) \geq 0 \\ v^{*,\text{mini}} & \text{else} \end{cases}$$

and $v^{*,\text{equi}}$ is given by (4.24). $v^{*,\text{mini}}$ is the unique solution of $Q(v) = 0$ over $[v_{\min}, v_{\max}]$.

Proof: All the proof ingredients have been given before. Note that $v^{*,\text{equi}}$ might be superior to v_{\max} . But since we have proved that $Q(v \geq v_{\max}) \leq 0$, this case does not have to be explicitly considered.

Note that this additional result can also be shown :

$$Q(v^{*,\text{equi}}) \geq 0 \Leftrightarrow \beta \geq 1 + \sqrt{5} \text{ or } \left(\beta^0 < \beta < 1 + \sqrt{5} \text{ and } \gamma \geq f(\beta) \right)$$

where β^0 is the root of the fourth order polynomial $16 - 16X - 4X^2 + X^4$ which approximate value is given by $\beta^0 \approx 2.77294$ and the fonction f is given by

$$f(\beta) = \frac{(\beta - 2)^3 \beta (\beta + 2) + (4 + 2\beta - \beta^2) \sqrt{-16 + 48\beta - 44\beta^2 + 12\beta^3 + 3\beta^4 - 4\beta^5 + \beta^6}}{16 - 16\beta - 4\beta^2 + \beta^4}$$

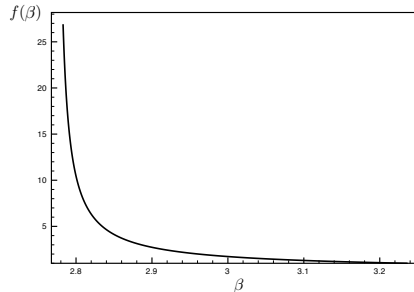


Figure 6: Switch from a 2 points to a 3 points equioscillations for $\beta^0 < \beta < 1 + \sqrt{5}$. The 3 points equioscillation occurs when $\gamma \geq f(\beta)$.

$f(\beta)$ for $\beta^0 < \beta < 1 + \sqrt{5}$ is plotted on figure 6. We can remark that $f(\beta) \geq 1, \forall \beta$ so that the condition $\gamma \geq f(\beta)$ is always false for $\gamma = 1$ (continuous case).

It is also interesting to know if $\chi = \sqrt{\frac{p_1 p_2}{2\gamma}} = 1$ is either a local minimum or a local maximum of the optimized convergence factor by looking at the sign of $\frac{\partial^2 \rho_{RR}^\dagger}{\partial \chi^2}(p_1, \chi)$. It can be proved that in terms of the variable $v = 2\gamma/p_1 - p_1$, the inequality $\frac{\partial^2 \rho_{RR}^\dagger}{\partial \chi^2}(p_1, \chi) > 0$ can be written:

$$v \geq v_0, \quad \text{where } v_0 = 2(\gamma - 1) + \sqrt{2(1 + \gamma^2)}$$

We deduce that $\zeta = \chi = 1$ is a local minimum only if $v^{*,\text{mini}} \leq v_0$. This can be checked by evaluating the polynomial $Q(v)$ in $v = v_0$ and looking at the sign of the result: if $Q(v_0) \leq 0$ then $v^{*,\text{mini}} \leq v_0$ and we have a local minimum at $\zeta = \chi = 1$.

It can be found that

$$Q(v_0) < 0 \Leftrightarrow 2 < \beta < \beta_0 \quad \text{or} \quad (\beta_0 \leq \beta \leq 2\sqrt{2} \text{ and } \gamma < g(\beta))$$

where $\beta_0 = \frac{8 + 5\sqrt{2}}{2(3 + 2\sqrt{2})} + \frac{\sqrt{90 + 64\sqrt{2}}}{2(3 + 2\sqrt{2})} \approx 2.44547$. The analytical expression of $g(\beta)$ is complicated and is not given here. Note that $g(\beta) \geq 1, \forall \beta$ so that, for the special case $\gamma = 1$, $Q(v_0) < 0$ is equivalent to $2 < \beta \leq 2\sqrt{2}$.

Figure 7 summarizes the three different domains: 3 points equioscillation, 2 points equioscillation with χ as a local maximum and 2 points equioscillation with χ as a local minimum.

The resulting optimized convergence factor is shown in figure 8 with respect to μ and γ .

We can draw the usual remarks about the convergence properties of the Schwarz algorithms : the convergence speed increases when the discontinuities of the coefficients (γ) is increased and the convergence speed decreases when μ , an increasing function of the ratio $\frac{\omega_{\max}}{\omega_{\min}}$, is increased.

In figures 9, 10 we compare, for $\mu = 2$ and $\mu = 6$, the results found in the two-sided case with the one of the section 3 for the *Robin-Neumann* transmission

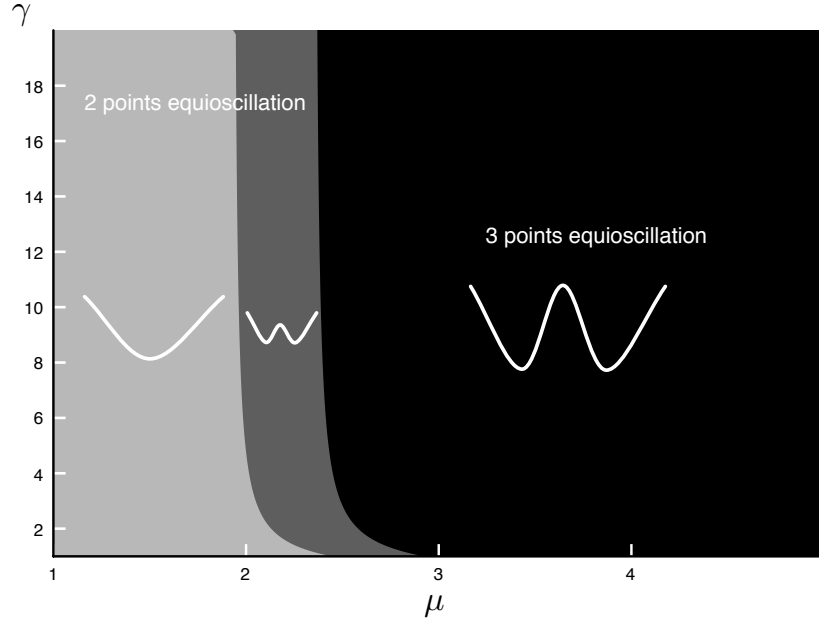


Figure 7: The three different domains of three points equioscillation (black), two points equioscillation with χ being a local maximum (dark grey) and two points equioscillation with χ being a local minimum (light grey)

conditions.

The *Robin-Robin* approach is highly more efficient than the *Robin-Neumann* approach when γ is closed to one. When γ is increased, the two approaches tends towards a *Dirichlet-Neumann* operator.

4.5 The continuous case

Theorem 4.5 (Continuous case) *Under the assumptions $D_1 = D_2 = D$, the optimal parameters p_1^* and p_2^* are given by*

$$\begin{cases} p_1^* = \frac{1}{2} \left[-v^* + \sqrt{8 + (v^*)^2} \right] \\ p_2^* = 2/p_1^* = p_1^* + v^* \end{cases}$$

where

$$v^* = \begin{cases} 2\sqrt{\beta-1} & \text{if } \beta \geq 1 + \sqrt{5} \\ \sqrt{2\beta^2 - 12} & \text{if } \sqrt{6} \leq \beta < 1 + \sqrt{5} \\ 0 & \text{if } 2 < \beta < \sqrt{6} \end{cases}$$

Proof: We use the theorem (4.4) which gives the optimal conditions in the general case.

As already mentioned the condition $Q(v^{*,\text{equi}}) \geq 0$ reduces for $\gamma = 1$ to $\beta \geq 1 + \sqrt{5}$. In that case, the solution of the minmax problem is given by $v^* = v^{*,\text{equi}} = 2\sqrt{\beta-1}$. If $\beta < 1 + \sqrt{5}$, we have to compute $v^{*,\text{min}}$ the value that cancels $Q(v)$ over

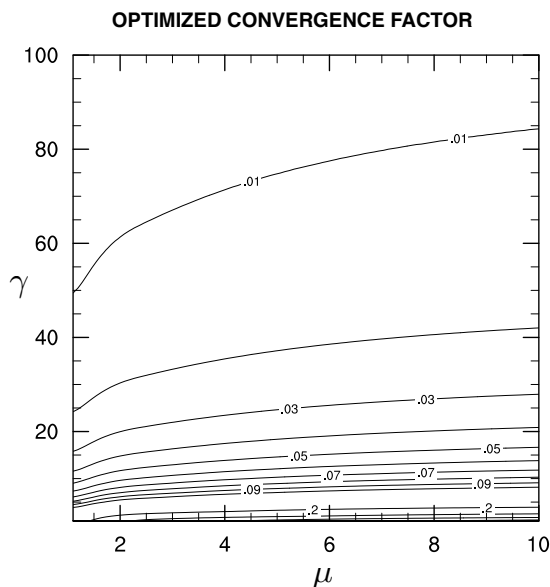


Figure 8: Optimized convergence factor with respect to μ and γ ($1 \leq \mu \leq 10, 1 \leq \gamma \leq 100$)

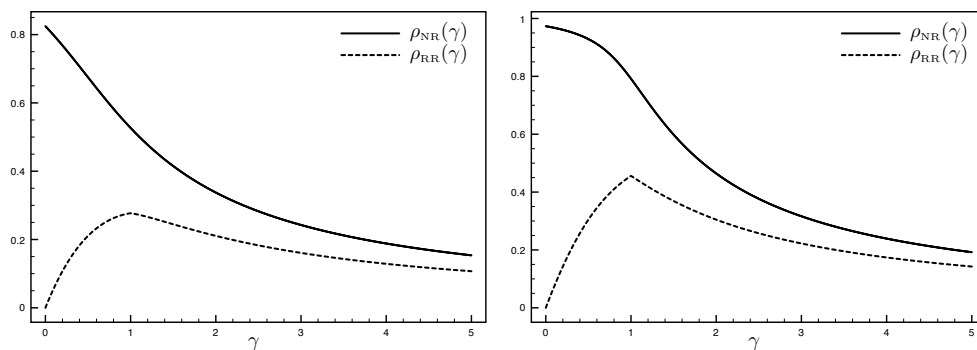


Figure 9: Optimized convergence factors for Neumann-Robin and Robin-Robin boundary conditions. $\mu = 2$ (left) and $\mu = 6$ (right)

$[v_{\min}, v_{\max}]$ where $v_{\min} = 0$, $v_{\max} = 2\sqrt{\beta^2 - 4}$.

For $\gamma = 1$, the expression (4.22) of the polynomial $Q(v)$ is

$$Q(v) = -\beta v (v^2 - (2\beta^2 - 12))$$

We find that

$$v^{*,\min} = \begin{cases} \sqrt{2\beta^2 - 12} & \text{if } \beta \geq \sqrt{6} \\ 0 & \text{if } 2 < \beta \leq \sqrt{6} \end{cases}$$

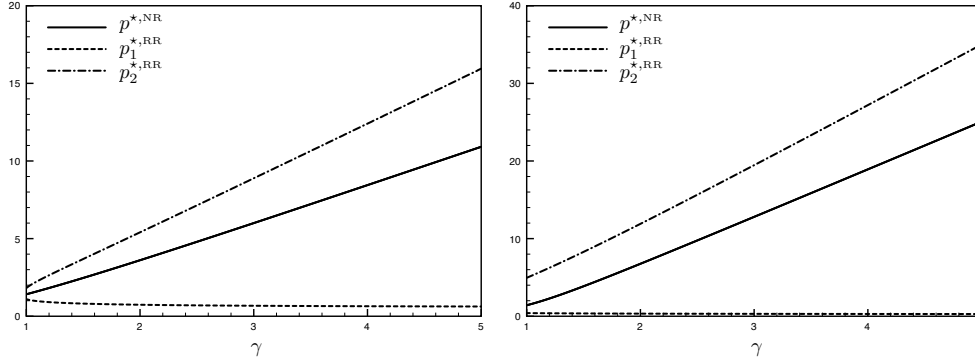


Figure 10: Optimized parameters for Neumann-Robin and Robin-Robin boundary conditions. $\mu = 2$ (left) and $\mu = 6$ (right)

Note that when $\beta \leq \sqrt{6}$, $v^* = 0$ which gives $p_1^* = p_2^* = \sqrt{2}$, which corresponds to the zeroth-order *one-sided* optimal parameters found in [10].

■

We have led so far a complete review of the convergence properties of the model problem (2.4) with constant coefficients. However we considered two subdomains with an infinite size, i.e. $L_1, L_2 \rightarrow \infty$. In the following section we intend to check the validity of this "infinite domain" assumption that is carried out during the convergence study of the algorithm. The aim is to validate the analytical formulae for the parameters p_1 and p_2 even with bounded subdomains.

5 Behaviour of Schwarz method with finite subdomains

As mentioned in section 2.2 to demonstrate and optimize the convergence of the Schwarz algorithm we classically make an "infinite domain" assumption which corresponds to suppose that errors go to zero only at infinite. However, when considering finite domains, we would like to be sure that the error vanishes on the bounded limit. The question we intend to address in this section is : what is the influence of subdomains finiteness on the optimal values of the Robin parameters in the interface conditions ?

5.1 Optimal symbols on bounded domains

We will consider two cases : first $\mathcal{B}_1 = \mathcal{B}_2 = Id$ and then $\mathcal{B}_1 = \mathcal{B}_2 = \partial_x$. Let us define $\lambda_j^{\text{opt,dd}}$ (resp. $\lambda_j^{\text{opt,nn}}$) the optimal symbols found with a Dirichlet condition (resp. Neumann condition). Without going into details, by carrying out a Fourier analysis of the model problem with a bounded domain, we can establish the following relations

$$\lambda_1^{\text{opt,dd}} = \lambda_1^{\text{opt},\infty} \coth \sqrt{i(\text{Fo}_2(\omega))^{-1}} \quad \lambda_2^{\text{opt,dd}} = \lambda_2^{\text{opt},\infty} \coth \sqrt{i(\text{Fo}_1(\omega))^{-1}} \quad (5.1)$$

in the Dirichlet case and

$$\lambda_1^{\text{opt,nn}} = \frac{\lambda_1^{\text{opt},\infty}}{\coth \sqrt{i(\text{Fo}_2(\omega))^{-1}}} \quad \lambda_2^{\text{opt,nn}} = \frac{\lambda_2^{\text{opt},\infty}}{\coth \sqrt{i(\text{Fo}_1(\omega))^{-1}}} \quad (5.2)$$

with $\lambda_1^{\text{opt},\infty}$ the symbols obtained by considering an infinite domain. The $\text{Fo}_j(\omega)$ terms are defined by $\text{Fo}_j(\omega) = \frac{D_j}{L_j^2 \omega}$. They are dimensionless, and can be related

to the well known Fourier number $\frac{D_j T}{L_j}$ which characterizes the heat conduction.

Note however that in our definition this quantity is a function of ω , instead of the characteristic time scale T . The aim of this section is now to determine, thanks to relations (5.1) and (5.2), whether the finiteness of subdomains significantly changes the value of the optimal symbols or not. We have then to compare $\lambda_j^{\text{opt,dd}}$, $\lambda_j^{\text{opt,nn}}$ and $\lambda_j^{\text{opt},\infty}$, i.e. to study the quantity $\coth \sqrt{i(\text{Fo}_j(\omega))^{-1}}$. By considering $\omega > 0$ we obtain following ratios

$$\begin{aligned} \frac{\Re(\lambda_1^{\text{opt,dd}})}{\Re(\lambda_1^{\text{opt},\infty})} &= \frac{\sinh(\sqrt{2}\text{Fo}_j^{-1/2}(\omega)) + \sin(\sqrt{2}\text{Fo}_j^{-1/2}(\omega))}{\cosh(\sqrt{2}\text{Fo}_j^{-1/2}(\omega)) - \cos(\sqrt{2}\text{Fo}_j^{-1/2}(\omega))} \\ \frac{\Im(\lambda_1^{\text{opt,dd}})}{\Im(\lambda_1^{\text{opt},\infty})} &= \frac{\sinh(\sqrt{2}\text{Fo}_j^{-1/2}(\omega)) - \sin(\sqrt{2}\text{Fo}_j^{-1/2}(\omega))}{\cosh(\sqrt{2}\text{Fo}_j^{-1/2}(\omega)) - \cos(\sqrt{2}\text{Fo}_j^{-1/2}(\omega))} \end{aligned} \quad (5.3)$$

We can now focus our attention on estimating the right hand side of those equations to find the values of Fourier numbers for which those terms significantly differ from one. Indeed as the couple (λ_1, λ_2) that cancels the convergence factor is unique the $\lambda_j^{\text{opt,dd}}$ and $\lambda_j^{\text{opt},\infty}$ values must be close to each other to validate the assumption. In figure 11 the evolution of the previous ratios between real and imaginary parts with respect to Fourier number is represented. When those ratios are close to 1 the influence of the finiteness of subdomains is not an impacting factor on the convergence speed of our algorithm. It is striking to realize that for both real and imaginary parts an empirical "critical" Fourier number appears ($\text{Fo}_c \approx 0.02$). Below this number we can consider that $\lambda_j^{\text{opt,dd}} = \lambda_j^{\text{opt,nn}} = \lambda_j^{\text{opt},\infty}$, as the maximum deviation found in this case is of the order of 0.003%. Above this number the optimal symbols significantly differ. For example, for $\text{Fo} = 0.5$, (resp. $\text{Fo} = 2$) we commit an error of about 30% (resp. 100%). For applications with thin subdomains and long term integrations this could become problematic. Actually what we do in practice is that we assume that the optimal symbol for ρ_∞ (2.14) is also optimal for ρ_{dd} . So the assumption consists in considering that $\rho_{dd}^\dagger = \rho_{dd}(\lambda_1^{\text{opt},\infty}, \lambda_2^{\text{opt},\infty})$ and $\rho_{nn}^\dagger = \rho_{nn}(\lambda_1^{\text{opt},\infty}, \lambda_2^{\text{opt},\infty})$ are sufficiently small. Those terms are represented figure 12 for a few typical values of the parameters D_j and L_j . More generally by studying the behaviour of ρ_{dd}^\dagger and ρ_{nn}^\dagger when increasing or decreasing the value of the parameters we get

$$\rho_{dd}^\dagger \rightarrow 0 \text{ for } D_j \rightarrow 0 \quad \rho_{dd}^\dagger \rightarrow 1 \text{ for } \omega \rightarrow 0 \quad \rho_{dd}^\dagger \rightarrow 1 \text{ for } L_j \rightarrow 0 \quad (5.4)$$

and similar results for ρ_{nn}^\dagger . This means that the dimensionless quantity $\text{Fo}_j(\omega) = \frac{D_j}{L_j^2 \omega}$ must be small enough to validate the infinite domain assumption.

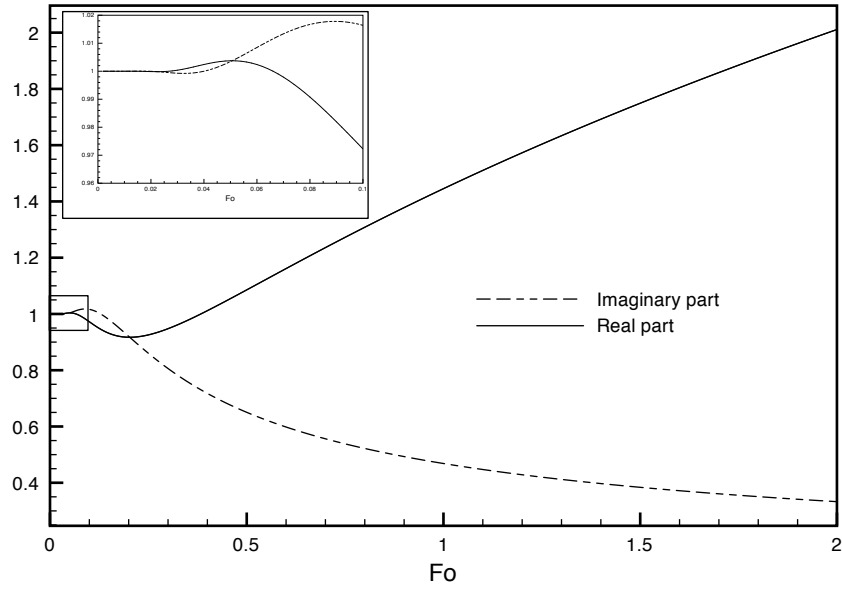


Figure 11: Evolution of the ratio, given by (5.3), between real parts and imaginary parts of optimal symbols $\lambda_j^{\text{opt},\text{dd}}$ and $\lambda_j^{\text{opt},\infty}$ with respect to Fourier number. A "critical value" appears to be $\text{Fo}_c = 0.02$.

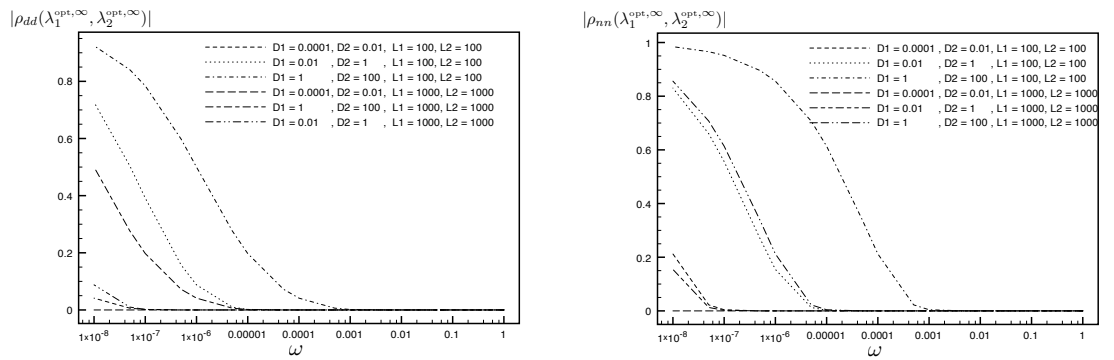


Figure 12: Behaviour of ρ_{dd}^\dagger and ρ_{nn}^\dagger with respect to ω for various values of D_j and L_j .

Note that in the continuous case $D_1 = D_2 = D$, we have

$$|\rho_{dd}^\dagger|_{cont} = |\rho_{nn}^\dagger|_{cont} = \exp\left(-\sqrt{2}(Fo_1^{-1} + Fo_2^{-1})\right) \quad (5.5)$$

which is less than 1, so the algorithm remains convergent. We have found so far a quantity useful to know whether the finiteness of subdomains is an impacting factor on optimal symbols of the Schwarz method. The study so far has been done in Fourier space. However it is interesting now to assess the impact of the finiteness of the subdomains on the optimized Robin parameters which are solution of (2.18).

5.2 Consequences for *Optimized Schwarz Methods*

We have suggested so far that the convergence factor ρ_∞ , usually used as a basis of the optimization problem (2.18), is probably not relevant in any cases. Following the analytical results found in section 4 for given values of D_j , ω_{min} and ω_{max} we are able to compute the optimal parameters p_1^* and p_2^* solution of (2.18) with $\rho = \rho_\infty$. In the situations where the "infinite domain" assumption is satisfied we should have $\rho_\infty(p_1^*, p_2^*) = \rho_{dd}(p_1^*, p_2^*) = \rho_{nn}(p_1^*, p_2^*)$. However, following the results of §5.1, for large values of the quantity $\frac{D_j}{\omega L_j^2}$ we should see that

this equality is no longer satisfied. To check the validity of those remarks we let $D_1 = 10^{-2}m^2.s^{-1}$, $D_2 = 1m^2.s^{-1}$, $L_1 = L_2 = 100m$ and $\omega_{max} = 1s^{-1}$. For two ranges of time frequencies (i.e. for two ranges of $Fo_j(\omega)$) we check the behaviour of $\rho_\infty(p_1^*, p_2^*)$, $\rho_{dd}(p_1^*, p_2^*)$ and $\rho_{nn}(p_1^*, p_2^*)$. The results, plotted on figure 13, are in good agreement with the results found in previous section and with figure 11. Indeed for low frequencies we see a divergence of the three functions and there is a transition from a region where $\rho_{nn}(p_1^*, p_2^*)$ is better than $\rho_{dd}(p_1^*, p_2^*)$ and $\rho_\infty(p_1^*, p_2^*)$ to a region where $\rho_{nn}(p_1^*, p_2^*)$ become significantly worst. Those results show that the "infinite domain" assumption must be considered with caution either in situations where low temporal frequencies are expected or in certain configurations where the geometry of the domain and the diffusion coefficients lead to a large value of $\frac{D_j}{\omega L_j^2}$.

Part III

The variable coefficients case

6 OSM for diffusion problems with spatially variable coefficients

As mentioned previously in the introduction of this report, the diffusion coefficient may be spatially variable to account for local effects (e.g. turbulent boundary layers) within subdomains. In practical applications (like in oceanography or meteorology) diffusion coefficients are likely to vary by a factor of 100 in the vertical direction. That is why we propose in this section a methodology to determine analytically the convergence factor for non constant diffusion coefficients, in the case of two subdomains. We will make the assumption that the

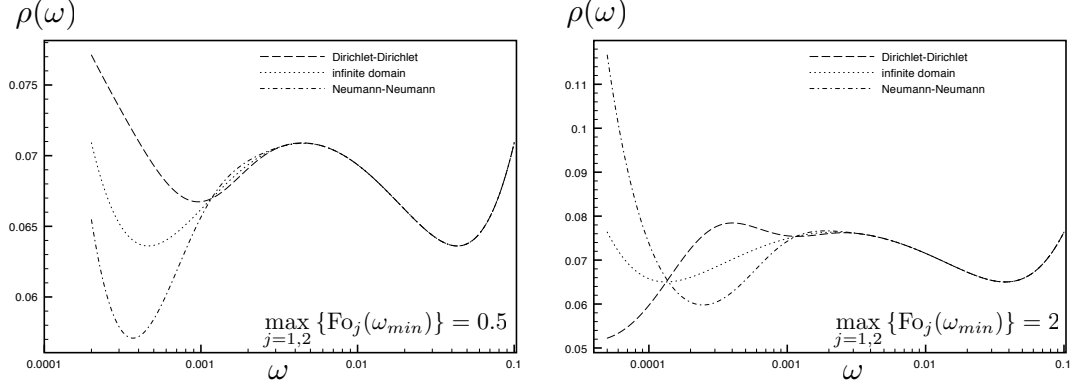


Figure 13: Behaviour of $\rho_\infty(p_1^*, p_2^*)$, $\rho_{dd}(p_1^*, p_2^*)$ and $\rho_{nn}(p_1^*, p_2^*)$ with respect to ω for $\omega_{max} = 1s^{-1}$, $D_1 = 10^{-2}m^2 \cdot s^{-1}$, $D_2 = 1m^2 \cdot s^{-1}$ and $L_1 = L_2 = 100m$. The value of ω_{min} is tuned to have $Fo_2(\omega_{min}) = 0.5$ (left panel) and $Fo_2(\omega_{min}) = 2$ (right panel). For $Fo_2(\omega_{min}) = 0.02$ the three convergence factor are exactly the same.

diffusion profile does not vary with time. The new model problem is 2.4 with $\mathcal{L}_j = \partial_t - \partial_x(D_j(x)\partial_x)$.

6.1 Analytical determination of the shape of the errors

The first part of our study does not require any distinction between subdomains, so the j subscripts are temporarily removed. If we denote by $g(t)$ the function containing the information given by the neighbouring subdomain, we intend to study the problem:

$$\begin{cases} \partial_t e - \partial_x(D(x)\partial_x e) = 0 & x \in]0, L[, t > 0 \\ e(x, 0) = 0 & x \in]0, L[\\ -D(0)\partial_x e(0, t) + p e(0, t) = g(t) & t > 0 \\ e(L, t) = 0 & t > 0 \end{cases} \quad (6.6)$$

with $p \in \mathbb{R}$ the Robin parameter we wish to determine to optimize the convergence speed. We decide to impose a Dirichlet condition at $z = L$, which corresponds to having $\mathcal{B}_1 = \mathcal{B}_2 = \text{Id}$ in (2.7).

First it is important to notice that the method based on a Fourier analysis commonly used to analytically determine the convergence factor, as described in §2.2, is not applicable to our model problem with variable coefficients. Indeed, in Fourier space we obtain the ODE $i\omega\hat{e} - \partial_x(D(x)\partial_x\hat{e}) = 0$. The associated boundary value problem in Fourier space appears to be at least as complicated as the original problem in physical space. That is why we propose to study directly the system (6.6).

We have to tackle with an initial boundary problem with nonhomogeneous

boundary conditions. First we transform this original problem with a homogeneous equation and nonhomogeneous boundary conditions into a problem with nonzero right-hand side but with homogeneous boundary conditions, by searching for a solution under the form $e(x, t) = \varphi(x, t) + U(x, t)$ with φ a lifting function satisfying the boundary conditions. The transformed problem reads

$$\begin{cases} \partial_t U - \partial_x (D(x) \partial_x U) = f(x, t) = -\partial_t \varphi + \partial_x (D(x) \partial_x \varphi) & x \in]0, L[, t > 0 \\ U(x, 0) = -\varphi(x, 0) & x \in]0, L[\\ -D(0) \partial_x U(0, t) + pU(0, t) = 0 & t > 0 \\ U(L, t) = 0 & t > 0 \end{cases} \quad (6.7)$$

The choice of φ is not unique. We choose this function as the solution of problem (6.6) with a constant diffusion coefficient whose value is the value at $x = 0$, i.e. φ is solution of

$$\begin{cases} \partial_t \varphi - D(0) \partial_{xx} \varphi = 0 & x \in]0, L[, t > 0 \\ -D(0) \partial_x \varphi(0, t) + p\varphi(0, t) = g(t) & t > 0 \\ \varphi(L, t) = 0 & t > 0 \end{cases} \quad (6.8)$$

Then we search for $U(x, t)$ under the form of a series with separate variables $U(x, t) = \sum_n \Phi_n(x) T_n(t)$. By substituting in (6.7) one gets

$$\sum_n T'_n(t) \Phi_n(x) - \sum_n T_n(t) \partial_x (D(x) \partial_x \Phi_n(x)) = f(x, t) \quad (6.9)$$

and we expand similarly the rhs into a series with respect to the functions $\Phi_n(x)$

$$f(x, t) = -\partial_t \varphi + \partial_x (D(x) \partial_x \varphi) = \sum_n f_n(t) \Phi_n(x) \quad (6.10)$$

The following step is now to properly choose the functions Φ_n . A relevant choice is supposed to enable us to transform the PDE into ODEs for unknown functions $\Phi_n(x)$ and $T_n(t)$. Therefore the natural choice for $\Phi_n(x)$ corresponds to the following *regular Sturm-Liouville* (SL) problem

$$\begin{cases} \partial_x (D(x) \partial_x \Phi_n) + \lambda_n^2 \Phi_n = 0 & x \in]0, L[\\ -D(0) \partial_x \Phi_n(0) + p \Phi_n(0) = 0 \\ \Phi_n(L) = 0 \end{cases} \quad (6.11)$$

with λ_n the eigenvalues of the SL operator. Such a choice leads to a family of functions $\Phi_n(x)$ which are orthonormal for the Euclidian scalar product $\langle u, v \rangle = \int_0^L u(x)v(x)dx$. The properties of regular SL problems are fully described in [15] or [1] and particular examples of the functions $\Phi_n(x)$ are shown in §7.2. After some simple algebra it turns out that a general solution of problem (6.6) is given by

$$e(x, t) = \varphi(x, t) + \sum_n \Phi_n(x) \int_0^t \exp(-\lambda_n^2(t - \tau)) f_n(\tau) d\tau \quad (6.12)$$

where φ satisfies (6.8), Φ_n satisfies (6.11) and $f_n(t)$ satisfies

$$f_n(t) = \int_0^L \partial_x (\tilde{D}(x) \partial_x \varphi) \Phi_n(x) dx \quad \text{with } \tilde{D}(x) = D(x) - D(0) \quad (6.13)$$

By formulating the solution of our problem under this form we can properly separate the error into two parts corresponding to two different contributions. Indeed $\varphi(x, t)$ corresponds to the error for a constant coefficient which value is $D(0)$ and $\sum_n \Phi_n(x) \int_0^t \exp(-\lambda_n^2(t - \tau)) f_n(\tau) d\tau$ represents the errors coming from the perturbations around $D(0)$, namely $\tilde{D}(x)$.

We must now determine explicitly the function φ which is part of $e(x, t)$ and which is also involved in the computation of $f_n(t)$. This is probably not relevant to try to solve (6.8) in physical space because it would result in expressing φ as a series, which would lead to a quite complicated expression for f_n 's as well as for $e(x, t)$. A more straightforward way consists in using the continuous Fourier transform. By taking into account the boundary conditions in 0 and L , one gets

$$\hat{\varphi}(x, \omega) = \frac{\left(e^{\sqrt{\frac{i\omega}{D(0)}}x} - e^{\sqrt{\frac{i\omega}{D(0)}}(2L-x)} \right)}{p \left(1 - e^{2\sqrt{\frac{i\omega}{D(0)}}L} \right) - \sqrt{i\omega D(0)} \left(1 + e^{2\sqrt{\frac{i\omega}{D(0)}}L} \right)} \hat{g}(\omega) \quad (6.14)$$

Since the inverse Fourier transform of this expression is very complicated to determine, the entire error (6.12) must be expressed in the Fourier space. The f_n 's are extended by zero for $t < 0$ and by the convolution theorem we have

$$\mathcal{F} \left\{ \int_0^t \exp(-\lambda_n^2(t - \tau)) f_n(\tau) d\tau \right\} = \hat{s}_n(\omega) \hat{f}_n(\omega) \quad \text{with } \hat{s}_n(\omega) = \mathcal{F} \left(e^{-\lambda_n^2 t} H(t) \right) = \frac{1}{\lambda_n^2 + i\omega}$$

where $H(t)$ is the Heaviside unit step function. The general form for $\hat{e}(x, \omega)$ is

$$\hat{e}(x, \omega) = \hat{\varphi}(x, \omega) + \sum_n \Phi_n(x) \hat{s}_n(\omega) \hat{f}_n(\omega) \quad (6.15)$$

In practice it is usually assumed that the subdomains are unbounded ($L \rightarrow \infty$) to simplify the expression of the convergence factor and thus to simplify the optimisation problem. By taking into account the results of section 5 concerning the effect of the finiteness of the subdomains on the optimal parameters, we assume that the quantity $\frac{\max_x D(x)}{L^2 \omega} \ll 1$. For applications in ocean and atmosphere, this is an acceptable assumption. The expression of $\hat{\varphi}$ can be then approximated by

$$\hat{\varphi}(x, \omega) \simeq \frac{\exp\left(-\sqrt{\frac{i\omega}{D(0)}}x\right)}{p + \sqrt{i\omega D(0)}} \hat{g}(\omega) \quad (6.16)$$

This implies

$$\hat{f}_n(\omega) \simeq \frac{\hat{g}(\omega)}{p + \sqrt{i\omega D(0)}} \int_0^L \frac{\partial}{\partial x'} \left(\tilde{D}(x') \frac{\partial}{\partial x'} \exp\left(-\sqrt{\frac{i\omega}{D(0)}}x'\right) \right) \Phi_n(x') dx' \quad (6.17)$$

Finally as a result of our study one can propose an expression for the error function in Fourier space that takes into account the spatial variability of the

diffusion coefficient:

$$\begin{aligned} \tilde{e}(x, \omega) \simeq & \frac{\hat{g}(\omega)}{p + \sqrt{i\omega D(0)}} \left[\exp\left(-\sqrt{\frac{i\omega}{D(0)}}x\right) \right. \\ & \left. + \sum_n \frac{\sqrt{\frac{i\omega}{D(0)}}\Phi_n(x)}{i\omega + \lambda_n^2} \int_0^L \tilde{D}(x') \exp\left(-\sqrt{\frac{i\omega}{D(0)}}x'\right) \frac{d\Phi_n}{dx'} dx' \right] \quad x \geq 0 \end{aligned} \quad (6.18)$$

This error has been constructed on the bounded domain $[0, L]$ which can be identified to subdomain Ω_2 , with the notations of section 2. For $x \in [-L, 0]$ (i.e. on Ω_1) we obtain a very similar form:

$$\begin{aligned} \tilde{e}(x, \omega) \simeq & \frac{\hat{h}(\omega)}{p + \sqrt{i\omega D(0)}} \left[\exp\left(\sqrt{\frac{i\omega}{D(0)}}x\right) \right. \\ & \left. - \sum_n \frac{\sqrt{\frac{i\omega}{D(0)}}\Phi_n(x)}{i\omega + \lambda_n^2} \int_{-L}^0 \tilde{D}(x') \exp\left(\sqrt{\frac{i\omega}{D(0)}}x'\right) \frac{d\Phi_n}{dx'} dx' \right] \quad x \leq 0 \end{aligned} \quad (6.19)$$

where the function h is the analogous of function g previously introduced.

The form of the error proposed in (6.18) is interesting because it is in good agreement with existing inferences about the impact of the spatial variability of coefficients on the convergence speed. Indeed, there exists such inferences in [5] based on a study of a two-dimensional steady-state diffusion problem. It is suggested that if we look at the diffusion coefficient only locally (i.e. the interface value) we are making a good approximation for high frequencies and a bad one for low frequencies. It is also inferred that neither the values of the diffusion coefficient far from the interface nor the boundary condition at $x = L_j$ are supposed to affect the convergence for high frequencies. Those intuitions are fully consistent with our analytical study. The term $\tilde{D}(x)$ which corresponds to the variability of the coefficient is weighted by $e^{-\sqrt{\frac{i\omega}{D(0)}}x}$ which makes this variability negligible for large values of ω but potentially significant for low frequencies. Moreover we can draw the same remark for the variations with x : when x is small (near the interface) $\tilde{D}(x)$ is weighted by a non negligible number while for x large enough $e^{-\sqrt{\frac{i\omega}{D(0)}}x}$ is almost zero.

6.2 Convergence factor of the *Dirichlet-Neumann* algorithm with spatially variable coefficients

We have established so far a general form for the errors propagating in each subdomain. We are now able to propose a formulation of the convergence speed for the global-in-time Schwarz algorithm with spatially variable coefficients. Before dealing with the general Robin-Robin case we intend to determine the convergence speed in a simpler Dirichlet-Neumann case, i.e. with the notations of section 2.1 $\mathcal{G}_j = \text{Id}$ and $\mathcal{F}_j = D_j(0)\frac{\partial}{\partial x}$. Moreover, for sake of practical convenience, we will try to find the expression of an "effective" value D_j^{eff} , which would be a constant value that would have the same effect on the convergence speed as the whole non constant diffusion profile $D_j(x)$. Hereafter we use again the subscripts j to characterize both subdomains.

A derivation very similar to what was done in section 6.1, but with a Dirichlet boundary condition instead of a Robin boundary condition leads to:

$$\widehat{e}_2(x, \omega) = \left(e^{-\sqrt{\frac{i\omega}{D_2(0)}}x} + \sum_n \sqrt{\frac{i\omega}{D_2(0)}} \frac{\Phi_{n,2}(x)}{i\omega + \lambda_{n,2}^2} \int_0^{L_2} \widetilde{D}_2(x') e^{-\sqrt{\frac{i\omega}{D_2(0)}}x'} \frac{d\Phi_{n,2}(x')}{dx'} dx' \right) \widehat{g}(\omega) \quad (6.20)$$

where $\widehat{g}(\omega) = \widehat{e}_1(0, \omega)$ and where the $\Phi_{n,2}$ are defined by a SL problem similar to (6.11), but again with a Dirichlet condition instead of a Robin condition. On Ω_1 , we have (by simply making $p = 0$ in the derivation of section 6.1):

$$\widehat{e}_1(x, \omega) = \left(e^{\sqrt{\frac{i\omega}{D_1(0)}}x} - \sum_n \sqrt{\frac{i\omega}{D_1(0)}} \frac{\Phi_{n,1}(x)}{i\omega + \lambda_{n,1}^2} \int_{-L_1}^0 \widetilde{D}_1(x') e^{\sqrt{\frac{i\omega}{D_1(0)}}x'} \frac{d\Phi_{n,1}(x')}{dx'} dx' \right) \frac{\widehat{h}(\omega)}{\sqrt{i\omega D_1(0)}} \quad (6.21)$$

where $\widehat{h}(\omega) = D_2(0) \frac{\partial \widehat{e}_2}{\partial x}(0, \omega)$ and where the $\Phi_{n,1}$ are defined by a SL problem similar to (6.11), but again with $p = 0$, i.e. with a Neumann condition instead of a Robin condition.

Therefore the multiplicative Schwarz algorithm with Dirichlet-Neumann conditions corresponds to having \widehat{e}_2^k and $\widehat{g}^k(\omega) = \widehat{e}_1^k(0, \omega)$ instead of \widehat{e}_2 and \widehat{g} in (6.20), and \widehat{e}_1^k and $\widehat{h}^{k-1}(\omega) = D_2(0) \frac{\partial \widehat{e}_2^{k-1}}{\partial x}(0, \omega)$ instead of \widehat{e}_1 and \widehat{h} in (6.21). So we have:

$$\begin{aligned} \widehat{g}^k(\omega) &= \left(1 - \sum_n \sqrt{\frac{i\omega}{D_1(0)}} \frac{\Phi_{n,1}(0)}{i\omega + \lambda_{n,1}^2} \int_{-L_1}^0 \widetilde{D}_1(x') e^{\sqrt{\frac{i\omega}{D_1(0)}}x'} \frac{d\Phi_{n,1}(x')}{dx'} dx' \right) \frac{1}{\sqrt{i\omega D_1(0)}} \widehat{h}^{k-1}(\omega) \\ \widehat{h}^k(\omega) &= \left(-1 + \sum_n \frac{\frac{d\Phi_{n,2}}{dx}(0)}{i\omega + \lambda_{n,2}^2} \int_0^{L_2} \widetilde{D}_2(x') e^{-\sqrt{\frac{i\omega}{D_2(0)}}x'} \frac{d\Phi_{n,2}(x')}{dx'} dx' \right) \sqrt{i\omega D_2(0)} \widehat{g}^k(\omega) \end{aligned} \quad (6.22)$$

Therefore, if we define a convergence rate by

$$\rho_{DN}^{var}(\omega) = \left| \frac{\widehat{e}_1^k(0, \omega)}{\widehat{e}_1^{k-1}(0, \omega)} \right| \quad (6.23)$$

the preceding relations lead to

$$\rho_{DN}^{var}(\omega) = \left| \frac{\widehat{g}^k}{\widehat{g}^{k-1}} \right| = \left| \frac{\widehat{g}^k}{\widehat{h}^{k-1}} \frac{\widehat{h}^{k-1}}{\widehat{g}^{k-1}} \right| = \rho_{DN}^{cst} \cdot \widetilde{\rho}_{DN} \quad (6.24)$$

where $\rho_{DN}^{cst} = \sqrt{\frac{D_2(0)}{D_1(0)}}$ is the convergence factor obtained in the case of constant diffusion coefficients (see [22]) and

$$\widetilde{\rho}_{DN} = \left| \left(1 - \sum_n \frac{\sqrt{\frac{i\omega}{D_1(0)}} \Phi_{n,1}(0)}{i\omega + \lambda_{n,1}^2} \int_{-L_1}^0 \widetilde{D}_1(x') e^{\sqrt{\frac{i\omega}{D_1(0)}}x'} \frac{d\Phi_{n,1}(x')}{dx'} dx' \right) \cdot \left(1 - \sum_n \frac{\frac{d\Phi_{n,2}}{dz}(0)}{i\omega + \lambda_{n,2}^2} \int_0^{L_2} \widetilde{D}_2(x) e^{-\sqrt{\frac{i\omega}{D_2(0)}}x} \frac{d\Phi_{n,2}(x)}{dx} dx \right) \right| \quad (6.25)$$

This result is interesting since we clearly see that the convergence factor ρ_{DN}^{var} is the product of the convergence factor with constant coefficients (the surface values) by a term coming from the spatial variability of the diffusion coefficient on Ω_1 and Ω_2 .

We can thus suggest "effective" constant values for D_1 and D_2 , which would have a similar effect on the convergence speed than the non constant vertical profiles $D_1(x)$ and $D_2(x)$, i.e. $\rho_{DN}^{var} = \sqrt{\frac{D_2^{eff}(\omega)}{D_1^{eff}(\omega)}}$ with

$$D_1^{eff}(\omega) = \frac{D_1(0)}{\left| 1 - \sum_n \frac{\sqrt{\frac{i\omega}{D_1(0)}} \Phi_{n,1}(0)}{i\omega + \lambda_{n,1}^2} \int_{-L_1}^0 \tilde{D}_1(x') e^{\sqrt{\frac{i\omega}{D_1(0)}} x'} \frac{d\Phi_{n,1}}{dx'}(x') dx' \right|^2} \quad (6.26)$$

and respectively

$$D_2^{eff}(\omega) = D_2(0) \left| 1 - \sum_n \frac{\frac{d\Phi_{n,2}}{dx}(0)}{i\omega + \lambda_{n,2}^2} \int_0^{L_2} \tilde{D}_2(x) e^{-\sqrt{\frac{i\omega}{D_2(0)}} x} \frac{d\Phi_{n,2}}{dx}(x) dx \right|^2 \quad (6.27)$$

It is important to note that, due to the variability of the coefficients, the convergence factor is a function of the time frequency ω whereas this dependency does not exist with constant coefficients.

6.3 Convergence factor of the *Robin-Robin* algorithm with spatially variable coefficients

In this section we determine the convergence factor ρ_{RR}^{var} in the more general case of Robin-Robin interface conditions. Thanks to (6.18) and (6.19), we can express \hat{e}_1 and \hat{e}_2 in a compact form for iterate k

$$\begin{cases} \hat{e}_1^k(\omega, 0) = \mathcal{K}_1(\omega, D_1(0), \Phi_{n,1}, \lambda_{n,1}, p_1) \hat{h}^{k-1} \\ \hat{e}_2^k(\omega, 0) = \mathcal{K}_2(\omega, D_2(0), \Phi_{n,2}, \lambda_{n,2}, p_2) \hat{g}^k \end{cases} \quad (6.28)$$

where $\hat{g} = -D_1(0)\partial_x \hat{e}_1(0, \omega) + p_2 \hat{e}_1(0, \omega)$ and $\hat{h} = D_2(0)\partial_x \hat{e}_2(0, \omega) + p_1 \hat{e}_2(0, \omega)$. The problem on the interface $x = 0$ is given by the relations

$$\begin{cases} (D_1(0)\partial_x + p_1) \hat{e}_1^k(0, \omega) = (D_2(0)\partial_x + p_1) \hat{e}_2^{k-1}(0, \omega) = \hat{h}^{k-1} \\ (-D_2(0)\partial_x + p_2) \hat{e}_2^k(0, \omega) = (-D_1(0)\partial_x + p_2) \hat{e}_1^k(0, \omega) = \hat{g}^k \end{cases} \quad (6.29)$$

By combining (6.28) and (6.29) one gets:

$$\begin{cases} D_1(0)\partial_x \hat{e}_1^k(0, \omega) = \hat{h}^{k-1} - p_1 \hat{e}_1^k(0, \omega) = (1 - p_1 \mathcal{K}_1) \hat{h}^{k-1} \\ -D_2(0)\partial_x \hat{e}_2^k(0, \omega) = \hat{g}^k - p_2 \hat{e}_2^k(0, \omega) = (1 - \mathcal{K}_2 p_2) \hat{g}^k \end{cases} \quad (6.30)$$

By substituting this in (6.29) we finally get a relation linking \hat{g} and \hat{h}

$$\begin{cases} \hat{g}^k = ((p_1 + p_2)\mathcal{K}_1 - 1) \hat{h}^{k-1} \\ \hat{h}^{k-1} = ((p_1 + p_2)\mathcal{K}_2 - 1) \hat{g}^{k-1} \end{cases} \quad (6.31)$$

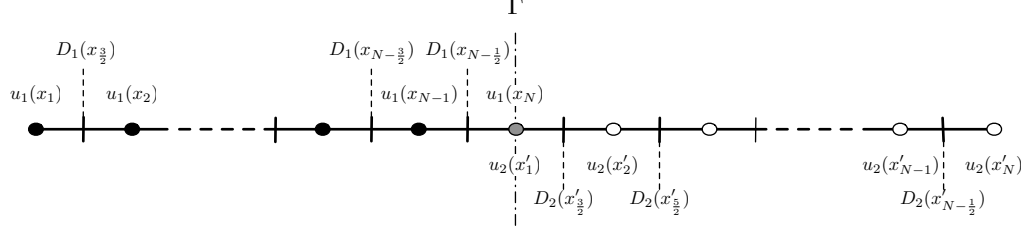


Figure 14: Spatial organisation and indexing of the numerical grid

which leads to the expression of the convergence factor:

$$\rho_{RR}^{var} = \left| \frac{\hat{g}^k}{\hat{g}^{k-1}} \right| = |[(p_1 + p_2)\mathcal{K}_1 - 1] [(p_1 + p_2)\mathcal{K}_2 - 1]| \quad (6.32)$$

The exact formulation of each term involved in the computation of ρ_{RR}^{var} is described appendix A.

We can note that this expression of the convergence factor is consistent with the expression (2.14) which was obtained in the case of constant (but discontinuous) coefficients. Indeed, if we set $\tilde{D}_1(x) = \tilde{D}_2(x) = 0$ in (2.14), we have then $\mathcal{K}_j = 1/\sqrt{i\omega D_j(0)}$, which leads to (2.14) (with $\lambda_j = p_j$ and $D_j\sigma_j^\pm = \pm\sqrt{i\omega D_j(0)}$).

7 Numerical results

In this section we intend to check numerically the validity of the theoretical results found in section 6. To do this, first, we describe the discretization of our model problem and then we design a few experiments to illustrate the relevancy of our approach.

7.1 Discretization and initial conditions

We choose to define two subdomains of equal sizes: $\Omega_1 = [-L, 0]$ and $\Omega_2 = [0, L]$. The model problem is discretized using a finite difference method on a staggered grid in space and an implicit scheme in time. Actually the discrete values of u are calculated at the centers of the cells, and the diffusion coefficients are located on the edges of the cells. The indexing is described on figure 14. The index for the values of u range from 1 to N , while the index for the values of the diffusion coefficient range from $\frac{3}{2}$ to $N + \frac{1}{2}$. The diffusion operator $\mathcal{D} = \frac{\partial}{\partial x} \left(D(x) \frac{\partial}{\partial x} \right)$ is discretized using the following second order formula for interior points:

$$\mathcal{D}_h u(x_i) = \frac{2}{h_{i+1} + h_i} \left[\frac{D(x_{i+1/2})}{h_{i+1}} (u(x_{i+1}) - u(x_i)) - \frac{D(x_{i-1/2})}{h_i} (u(x_i) - u(x_{i-1})) \right] \quad (7.33)$$

with $h_i = x_i - x_{i-1}$.

The interface conditions at $x = 0$ are discretized as follows:

$$g = -\frac{D_1(x_N)}{h_N}(u_1(x_N) - u_1(x_{N-1})) + p_1 u_1(x_N) \quad h = \frac{D_2(x'_1)}{h'_1}(u_2(x'_2) - u_2(x'_1)) + p_2 u_2(x'_1) \quad (7.34)$$

with x'_i the grid points on subdomain Ω_2 .

We must provide an initial condition to our model problem. In order to fulfill the assumption made for the convergence study, this initial condition must satisfy the compatibility conditions (i.e. the equality of the values and of the normal fluxes) at $x = 0$. This can be done by considering for instance the functions

$$u_1(x, 0) = 20 + e^{\frac{x}{a_1}} \quad u_2(x, 0) = 22 - e^{-\frac{x}{a_2}} \quad \text{with } \frac{a_1}{a_2} = \frac{D_1(0)}{D_2(0)} \quad (7.35)$$

The first iteration of the Schwarz algorithm requires to provide a first guess for $h^0(t) = (D_2(0)\partial_x u_2^0 + p_1 u_2^0)(0, t)$. We choose a random function following a uniform law, in order to generate a wide range of the temporal frequencies allowed by our temporal grid.

Finally we have to choose the functions $D_j(x)$ to complete the definition of our model problem. We will propose in the following two kinds of configurations.

7.2 Testcase # 1

Let us consider first a configuration with a constant coefficient D_1 on Ω_1 and a variable coefficient $D_2(x) = (1 + 3x)^{4/3}$ on Ω_2 . This particular profile was chosen because it makes it possible to solve analytically the regular Sturm-Liouville problem (6.11) and to avoid the pitfalls of the numerical evaluation of eigenvalues and eigenfunctions.. In the case of *Dirichlet-Neumann* conditions, like in §6.2, we have a Dirichlet condition in Ω_2 , and the eigenvalues $\lambda_{n,2}$ and eigenfunctions $\Phi_{n,2}$ associated to $D_2(x)$ are

$$\Phi_{n,2}(x) = \sqrt{\frac{2}{(1+3L)^{1/3} - 1}} \left(\frac{\sin(\lambda_{n,2}((1+3x)^{1/3} - 1))}{(1+3x)^{1/3}} \right) \quad \lambda_{n,2} = \frac{n\pi}{(1+3L)^{1/3} - 1} \quad (7.36)$$

The ten first eigenfunctions $\Phi_{n,2}(x)$ are shown on figure 15. We have used $n_{max} = 50$ eigenfunctions in our actual calculations.

As described in §6.2 it is possible to find a spatially constant value D_j^{eff} which has the same effect as the spatially variable profile $D_j(x)$ on the convergence speed. Those values appear naturally when considering a *Dirichlet-Neumann* case. We propose to study the evolution of the effective value D_2^{eff} with respect to the time frequencies ω . The expression of $D_2^{eff}(\omega)$ is given by (6.27). Values for $D_2^{eff}(\omega)$ are represented on figure 16. First we clearly see that the use of constant values (typically the surface values) to perform the convergence study in the case of spatially variable coefficients is not a reasonable assumption here, since the effective diffusion coefficient significantly differs from $D_2(0)$. For high temporal frequencies, we can consider $D_2(0) \approx D_2^{eff}(\omega)$. However this equality is far from being satisfied for low frequencies.

In order to validate this purely analytical result, we have to check it numerically. Let us discretize the one dimensional model problem using the finite

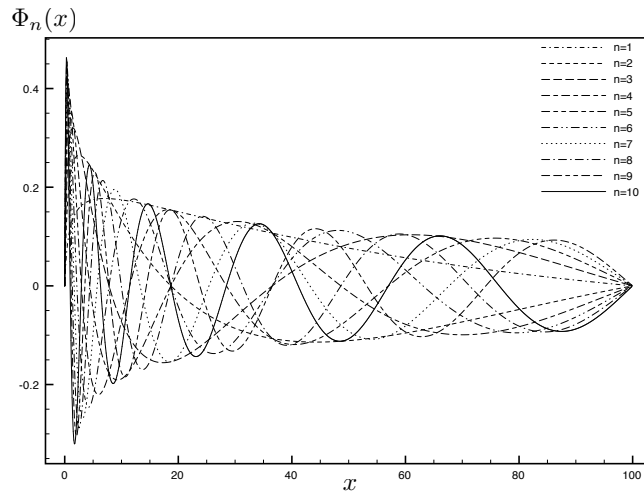


Figure 15: Ten first eigenfunctions $\Phi_{n,2}$ for $L = 100$.

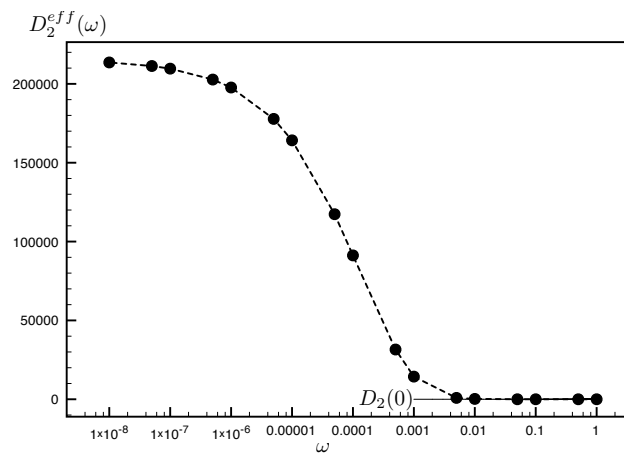


Figure 16: Evolution of D_2^{eff} with respect to ω , for $D_2(x) = (1 + 3x)^{4/3}$.

$\omega_{min}(s^{-1})$	1	10^{-1}	10^{-2}	10^{-3}	10^{-4}	10^{-5}
$\omega_{max}(s^{-1})$	10	1	10^{-1}	10^{-2}	10^{-3}	10^{-4}
$D_2^{eff}(m^2.s^{-1})$	2.5	14.5	54.5	62	62	62

Table 1: Numerical values of D_2^{eff} for various ranges of temporal frequencies.

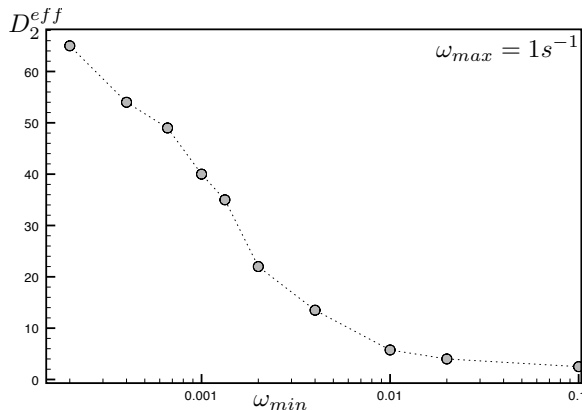


Figure 17: Evolution of D_2^{eff} with respect to ω_{min} . For this numerical study ω_{max} is kept constant and ω_{min} varies to cover a wide range of temporal frequencies.

difference approach described in §7.1 with $D_2(x) = (1 + 3x)^{4/3}$. The strategy to compute numerically the effective value of $D_2(x)$ is to consider a tunable value for the constant coefficient D_1 . We start from a very small value of D_1 which results in a divergent algorithm because $\rho_{DN}^{var} = \sqrt{\frac{D_2^{eff}(\omega)}{D_1}} \geq 1$. Then we increase D_1 until reaching a value for which the algorithm becomes convergent, which means that D_1 attained the value of $D_2^{eff}(\omega)$. The results are shown in table 1, in which the ratio $\omega_{max}/\omega_{min}$ is kept constant and equal to 10. They are consistent with our analytical study, as for high frequencies the value of $D_2^{eff}(\omega)$ has the same order of magnitude than $D_2(0)$ ($D_2(0) = 1$, $D_2^{eff}(\omega) = 2.5$). On the contrary for low frequencies the effective value increases until reaching a threshold at $D_2^{eff} = 62$. A quite similar result is represented on figure 17: the value of ω_{max} is kept constant while ω_{min} varies and the same kind of behaviour is observed.

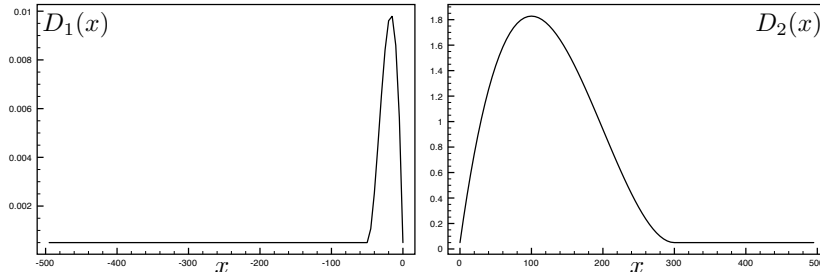
It should be noted that our validation is only qualitative and not quantitative. Indeed our discretized problem is not supposed to contain the same eigenvalues and eigenfunctions as those determined in the case of a continuous problem in our analytical study. On top of that our theoretical work carries a certain amount of assumptions concerning the shape of the error function because we considered $T \rightarrow \infty$ and $L_j \rightarrow \infty$.

Let us consider now the same kind of study but with *Robin-Robin* interface conditions (see §6.3). First we propose to check if the effective values found (nu-

ω_{min}	ω_{max}	number of iterations		
		(cst)	(eff)	(var)
10^{-1}	1	7	7	6
10^{-2}	10^{-1}	7	7	7
10^{-3}	10^{-2}	7	5	6
10^{-4}	10^{-3}	8	4	6
10^{-5}	10^{-4}	9	5	7
10^{-6}	10^{-5}	14	6	9

Table 2: Number of iterations to reach a tolerance of 10^{-4} (the convergence criteria is defined as the \mathcal{L}^2 -norm of the difference between two successive iterates), with $L_1 = L_2 = 100m$ and 100 points in each subdomain. Different kinds of optimal parameters corresponding to different kinds of optimization are considered. (cst) and (eff) correspond to an optimization with constant coefficients respectively with the interface values and with the effective values, and (var) is the result of the optimization for variable coefficients.

merically) in table 1 in the *Dirichlet-Neumann* case are still valid for a *Robin-Robin* case. Note that those effective values may not be appropriate with Robin conditions because they have been determined with Dirichlet or Neumann type boundary conditions. We therefore compute $p_1^{*,cst}$ and $p_2^{*,cst}$ which are solutions of (2.18) with $\rho = \rho_{RR}^{cst}$ and $D_2 = D_2(0)$. Similarly we compute $p_1^{*,eff}$ and $p_2^{*,eff}$ solutions of the minmax problem with $D_2 = D_2^{eff}$. Both optimization problems corresponding to the determination of $p_j^{*,cst}$ and $p_j^{*,eff}$ have an analytical solution given in §4.4. The results in table 2 show that the effective values found in a *Dirichlet-Neumann* case are still relevant. This suggests that, for our configuration, the eigenvalue problem (6.11) is not very sensitive to the type of boundary condition at $x = 0$. For low frequencies the convergence speed is significantly improved with the effective value due to the fact that D_j^{eff} significantly differ from $D_j(0)$. For this configuration we have also computed numerically the optimal parameters $p_1^{*,var}$ and $p_2^{*,var}$ solution of (2.18) with $\rho = \rho_{RR}^{var}$. The set of eigenvalues and eigenfunctions solution of (6.11), required to compute ρ_{RR}^{var} , is determined thanks to a simple matrix method based on the finite difference scheme (7.33). The convergence speed obtained with $p_1^{*,var}$ and $p_2^{*,var}$ is substantially the same than the one with effective values, which is an interesting feature for our approach. While the convergence speed deteriorates with low temporal frequencies when considering an optimisation with $D_2(x) = D_2(0)$ we robustly keep a fast convergence by taking into account the variability of the coefficients. Note that the effective values have been numerically found, these values have therefore been determined on the "true" frequency spectra $[\omega_{min}^*, \omega_{max}^*]$ of the simulation. In the same time the $p_1^{*,var}$ and $p_2^{*,var}$ values are the solution of an optimisation problem on a theoretical frequency spectra $[\omega_{min} = \frac{\pi}{\Delta t}, \omega_{max} = \frac{\pi}{T}]$ which may be quite different from $[\omega_{min}^*, \omega_{max}^*]$. The parameters $p_1^{*,eff}$ and $p_2^{*,eff}$ are the result of an optimisation on diffusion coefficients that are representative of the computational code whereas $p_1^{*,var}$ and $p_2^{*,var}$ are the result of an optimisation on diffusion coefficients coming from a continuous analysis. This is an explanation of the fact that the convergence is always faster with effective values.

Figure 18: Evolution of D_2 and D_1 with respect to x .

7.3 Testcase # 2: parabolic diffusion profiles

In the previous section we have considered a configuration with a constant diffusion coefficient on Ω_1 and a quasi-linear diffusion profile on Ω_2 . We propose now to investigate a more realistic case, in which the spatial variability of the diffusion coefficients is typical of a fluid with a turbulent boundary layer. This kind of profile is fully described in [23] and [16] for example. By evading all the physical details we can consider

$$D_j(x) = A_j x \left(1 - \frac{x}{h_{bl,j}}\right)^2 + \kappa_j \quad x \in [0, h_{bl,j}] \quad (7.37)$$

where $h_{bl,j}$ is the size of the boundary layer. Outside this boundary layer, i.e. for $x > h_{bl,j}$, the profile is constant and equal to κ_j (Note that we have a \mathcal{C}^1 continuity at $x = h_{bl,j}$ between the parabolic profile and the constant value). The terms A_j are constant values. We set $\kappa_1 = 0.0005 m^2 \cdot s^{-1}$, $\kappa_2 = 0.05 m^2 \cdot s^{-1}$, $h_{bl,1} = 50 m$, $h_{bl,2} = 300 m$, $A_1 = 0.004 m \cdot s^{-1}$, $A_2 = 0.04 m \cdot s^{-1}$, those values are chosen to be as representative as possible for real configurations in the oceanic and atmospheric context. The corresponding profiles are represented on figure 18. For our testcase we choose $L_1 = L_2 = 500 m$ and $dx_1 = dx_2 = 5$. Note that in practice the diffusion profile varies with respect to the surface fluxes (involved in the computation of $h_{bl,j}$) and to the distance from the interface. We consider here that the boundary layer size is constant by neglecting the impact of the surface flux on the diffusion profile, therefore the latter varies only with respect to x . We propose to study this testcase on various ranges of temporal frequencies. The corresponding convergence results are described in table 3. We have investigated different kind of Robin parameters, namely $p_1^{*,cst}$ and $p_2^{*,cst}$ for (cst) and $p_1^{*,var}$ and $p_2^{*,var}$ for (var). It is relatively surprising and unusual to realize that the convergence is faster for low frequencies. To explain this, it is useful to have a look at the effective values associated to $D_j(x)$. We implement the same strategy as the one proposed in §7.2 to compute numerically the effective values by mean of a *Dirichlet-Neumann* algorithm. These effective values are shown in table 4. Let us define the ratio $\gamma^{cst} = \frac{D_2(0)}{D_1(0)}$ corresponding to the jump between the diffusion coefficients at the interface. In our testcase we have $\gamma^{cst} = \frac{0.05}{0.0005} = 100$. This quantity is particularly interesting since it has a

		number of iterations	
ω_{min}	ω_{max}	(cst)	(var)
10^{-2}	10^{-1}	10	8
10^{-3}	10^{-1}	9	6
10^{-4}	10^{-1}	8	6
10^{-3}	10^{-2}	7	6
10^{-4}	10^{-2}	7	6
10^{-5}	10^{-2}	6	6
10^{-5}	10^{-4}	5	5
10^{-6}	10^{-4}	6	5
10^{-7}	10^{-4}	6	6

Table 3: Number of iterations to reach a tolerance of 10^{-4}

		effective values		
ω_{min}	ω_{max}	D_1^{eff}	D_2^{eff}	γ^{eff}
10^{-2}	10^{-1}	0.00051	0.051	100
10^{-3}	10^{-1}	0.00051	0.056	110
10^{-4}	10^{-1}	0.00055	0.11	200
10^{-3}	10^{-2}	0.00051	0.065	127
10^{-4}	10^{-2}	0.00052	0.1	192
10^{-5}	10^{-2}	0.0006	0.3	500
10^{-5}	10^{-4}	0.00075	0.4	533
10^{-6}	10^{-4}	0.0015	0.5	333
10^{-7}	10^{-4}	0.0025	0.7	280

Table 4: Effective values of $D_1(x)$ and $D_2(x)$ and their ratio $\gamma^{eff} = D_2^{eff}/D_1^{eff}$.

direct impact on the convergence speed. Following the results of §4.4 we know that the convergence speed is improving when γ^{cst} is increasing, i.e. $\rho_{RR}^{cst} \rightarrow 0$ when $\gamma^{cst} \rightarrow \infty$. In table 4 we see that γ^{eff} is larger than γ^{cst} for a wide range of temporal frequencies. This means that the spatial variability of the diffusion coefficients tends to improve the convergence speed of the associated algorithm. Indeed this acts to increase the discontinuity at the interface especially for low frequencies. The deterioration of the convergence due to low temporal frequencies is compensated by an increasing jump of the effective values at the interface. Moreover we see that for small values of the interface coefficient, $D_1(0)$ here, the effective value $D_1^{eff}(\omega)$ remains close to $D_1(0)$. This is consistent with formulae (6.27) and this is due to the term $e^{-\sqrt{\frac{i\omega}{D_1(0)}}x}$ which is extremely small for $D_1(0)$ small.

Concerning the optimization of ρ_{RR}^{var} it is interesting to see that it always performs at least as well as the optimisation of ρ_{RR}^{cst} . This shows that the optimisation tends to correct the values $p_1^{*,cst}$ and $p_2^{*,cst}$, used as first guesses of the numerical optimization, in a proper way.

8 Conclusion

In this report we studied the global-in-time Schwarz method for the coupling between two diffusion equations defined on two non-overlapping subdomains. In the first part we described the optimized version of this algorithm. In the second part we introduced a new optimized Schwarz method for non-overlapping diffusion problems with discontinuous coefficients. This method uses zeroth order two-sided Robin transmission conditions i.e. we considered two different Robin conditions on both sides of the interface. We based our approach on a model problem with two subdomains, we proved the convergence of the corresponding algorithm and we analytically studied the behaviour of the convergence factor with respect to the parameters of the problem. We showed that the optimized convergence factor satisfies an equioscillation property between two or three points depending on the configurations. In the case with continuous coefficients the performances obtained with a two-sided optimization are proved to be always at least as good as the one with a one-sided optimization i.e. with the same parameter in the Robin transmission conditions.

Finally, in the third part, we presented and analyzed a new approach to study the convergence of a global-in-time Schwarz algorithm in the case of a 1-D diffusion equation with variable coefficients. We showed that, thanks to our formulation, we are able to have a better understanding of the behaviour of the convergence factor. We exhibited some interesting features that were not shown by usual convergence studies with constant diffusion coefficients. We put particular emphasis on the fact that for low temporal frequencies it can be a strong (and irrelevant) assumption to assimilate a variable diffusion coefficient to its constant interface value. Moreover we also showed that the variability of the coefficients can have a positive feedback on the convergence speed by increasing the discontinuity at the interface.

However the formulae we got involve the computation of a set of eigenvalues and associated eigenfunctions which makes it "uncomfortable" to use in practice. On top of that the use of a numerical resolution of the minmax problem seems mandatory because the expression of the convergence factor is complex and prevents from an analytical resolution of the optimisation problem. To become attractive for practical applications our approach must be complemented to provide effective values independent of the eigenvalues and the eigenfunctions. This could be possible by performing an accurate study of the eigenvalues problems to improve our knowledge of the behaviour of the eigenvalues with respect to the diffusion profiles variations. An alternative could also be to proceed to an offline calculation of a set of effective values associated to a given family of relevant diffusion profiles and to pick in this set during the online computation.

References

- [1] **P. B. Bailey, W. N. Everitt, A. Zettl.** Regular and singular Sturm-Liouville problems with coupled boundary conditions. *Proc. Roy. Soc. Edinburgh*, 126A, 505-514, 1996.
- [2] **D. Bennequin, M.J. Gander and L. Halpern.** A homographic best approximation problem with application to optimized Schwarz waveform relaxation *to appear in Mathematics of Computation*, 2008
- [3] **E. Blayo, L. Halpern and C. Japhet.** Optimized schwarz waveform relaxation algorithms with nonconforming time discretization for coupling convection-diffusion problems with discontinuous coefficients. *Domain Decomposition Methods in Science and Engineering XVI; Series: Lecture Notes in Computational Science and Engineering*, 55, 2007.
- [4] **G. Danabasoglu, W. G. Large, J. Tribbia, P. Gent, B. Briegleb and J. C. McWilliams.** Diurnal coupling in the tropical oceans of ccm3. *Journal of climate*, Vol. 19, 2006
- [5] **O. Dubois.** Optimized schwarz methods for the advection-diffusion equation and for problems with discontinuous coefficients. *Ph.D. thesis, McGill University*, 2007.
- [6] **V. W. Ekman.** On the influence of the earth's rotation on ocean currents. *Arch. Math. Astron. Phys.*, 2, 1-52, 1905.
- [7] **B. Engquist and A. Majda.** Absorbing boundary conditions for the numerical simulation of waves. *Math. Comp.*, Vol. 31, pages 629-651, 1977.
- [8] **M. J. Gander and A. M. Stuart.** Space-Time Continuous Analysis of Waveform Relaxation for the Heat Equation. *SIAM Journal on Scientific Computing*, 19:2014-2031, 1998.
- [9] **M. J. Gander, L. Halpern and F. Nataf.** Optimized Schwarz methods. *In T. Chan, T. Kako, H. Karawada, and O. Pironneay, editors, Twelfth International Conference on Domain Decomposition Methods, Chiba, Japan*, pages 15-28, Bergen, 2001. Domain Decomposition Press.
- [10] **M. J. Gander and L. Halpern.** Methodes de relaxation d'ondes pour l'equation de la chaleur en dimension 1. *C. R. Acad. Sci. Paris t. 336, Série I*, pages 519-524, 2003.
- [11] **M. J. Gander and L. Halpern.** Optimized schwarz waveform relaxation for advection reaction diffusion problems. *SIAM Journal on Numerical Analysis*, 45(2):666-697, 2007.
- [12] **M.J. Gander and , L. Halpern, and F. Magoules.** An Optimized Schwarz Method with Two-Sided Robin Transmission Conditions for the Helmholtz Equation *Int. J. for Num. Meth. in Fluids*, Vol. 55, No. 2, pp. 163-175, 2007

- [13] **L. Halpern M. J. Gander and M. Kern.** A schwarz waveform relaxation method for advection-diffusion-reaction problems with discontinuous coefficients and non-matching grids. *Proceedings of the 16th International Conference on Domain Decomposition Methods*, 2005.
- [14] **C. Japhet and F. Nataf.** The best interface conditions for domain decomposition methods : Absorbing boundary conditions. *Artificial boundary conditions, with Applications to Computational Fluid Dynamics Problems*, L. Tournette eds, 2000.
- [15] **Q. Kong and A. Zettl.** Eigenvalues of regular Sturm-Liouville problems. *J. Differential Equations*, v. 131, no.1, 1-19, 1996.
- [16] **W. G. Large, J. C. McWilliams and S. C. Doney.** Oceanic Vertical Mixing: A Review and a Model with a Nonlocal Boundary Layer Parameterization. *Reviews of Geophysics*, Vol. 32, no. 4, pages 363-403, 1994.
- [17] **E. Lelarsmee, A. Ruehli and A. Sangiovanni-Vincentelli.** The waveform relaxation method for time-domain analysis of large scale integrated circuits *IEEE Trans. on CAD of IC and Syst.*, vol 1, pp 131-145, 1982
- [18] **P.L. Lions.** On the schwarz alternating method iii: a variant for nonoverlapping subdomains. In *Tony F. Chan, Roland Glowinski, Jacques Priaux, et Olof Widlund, Third International Symposium on Domain Decomposition Methods for Partial Differential Equations, held in Houston, Texas, March 20-22, 1990.*
- [19] **Y. Maday, F. Magoulés.** Non-overlapping additive Schwarz methods tuned to highly heterogeneous media *Comptes Rendus de l'Academie des Sciences. Serie 1, Mathematique 341-11 (2005) 701-705*
- [20] **O. S. Madsen.** A realistic model of the wind-induced Ekman boundary layer. *J. Phys. Oceanogr.*, 7, 248-255, 1977
- [21] **F. Nataf, F. Rogier and E. de Sturler.** Optimal interface conditions for domain decomposition methods. *Tech. Rep. 301, CMAP (Ecole Polytechnique)*, 1994.
- [22] **A. Quarteroni and A. Valli.** Domain Decomposition Methods for Partial Differential Equations. *Oxford Science Publications*, 1999
- [23] **Troen, I. and L. Mahrt.** A simple model of the atmospheric boundary layer: Sensitivity to surface evaporation. *Bound.-Layer Meteorol.*, 37, 129-148, 1986.

A Determination of the convergence rate in the case of variable coefficients

We recall (6.32):

$$\rho = |[(p_1 + p_2)\mathcal{K}_1 - 1] [(p_1 + p_2)\mathcal{K}_2 - 1]| \quad (1.38)$$

with

$$\begin{cases} \mathcal{K}_1 &= \left(1 - \sum_n \frac{\sqrt{\frac{i\omega}{D_1(0)}} \Phi_{n,1}(0)}{i\omega + \lambda_{n,1}^2} \int_{-L_1}^0 \tilde{D}_1(x) \exp\left(\sqrt{\frac{i\omega}{D_1(0)}} x\right) \frac{d\Phi_{n,1}}{dx} dx \right) \frac{1}{p_1 + \sqrt{i\omega D_1(0)}} \\ \mathcal{K}_2 &= \left(1 + \sum_n \frac{\sqrt{\frac{i\omega}{D_2(0)}} \Phi_{n,2}(0)}{i\omega + \lambda_{n,2}^2} \int_0^{L_2} \tilde{D}_2(x) \exp\left(-\sqrt{\frac{i\omega}{D_2(0)}} x\right) \frac{d\Phi_{n,2}}{dx} dx \right) \frac{1}{p_2 + \sqrt{i\omega D_2(0)}} \end{cases}$$

(1.38) can be rewritten as:

$$\rho = \sqrt{\left(\mathcal{I}m(\mathcal{K}_1)^2(p_1 + p_2)^2 + [(p_1 + p_2)\mathcal{R}e(\mathcal{K}_1) - 1]^2\right) \left(\mathcal{I}m(\mathcal{K}_2)^2(p_1 + p_2)^2 + [(p_1 + p_2)\mathcal{R}e(\mathcal{K}_2) - 1]^2\right)} \quad (1.39)$$

In order to determine the real and imaginary parts of \mathcal{K}_1 and \mathcal{K}_2 , we can decompose each term appearing in the preceding expressions:

- $a_j = \mathcal{R}e\left(\frac{\sqrt{\frac{i\omega}{D_j(0)}}}{i\omega + \lambda_{n,j}^2}\right) = \sqrt{\frac{\omega}{2D_j(0)}} \left(\frac{\lambda_{n,j}^2 + \omega}{\omega^2 + \lambda_{n,j}^4}\right)$
- $b_j = \mathcal{I}m\left(\frac{\sqrt{\frac{i\omega}{D_j(0)}}}{i\omega + \lambda_{n,j}^2}\right) = \sqrt{\frac{\omega}{2D_j(0)}} \left(\frac{\lambda_{n,j}^2 - \omega}{\omega^2 + \lambda_{n,j}^4}\right)$
- $c_1 = \mathcal{R}e\left(\exp\left(\sqrt{\frac{i\omega}{D_1(0)}} x\right)\right) = \cos\left(\sqrt{\frac{\omega}{2D_1(0)}} x\right) \exp\left(\sqrt{\frac{\omega}{2D_1(0)}} x\right)$
- $d_1 = \mathcal{I}m\left(\exp\left(\sqrt{\frac{i\omega}{D_1(0)}} x\right)\right) = \sin\left(\sqrt{\frac{\omega}{2D_1(0)}} x\right) \exp\left(\sqrt{\frac{\omega}{2D_1(0)}} x\right)$
- $c_2 = \mathcal{R}e\left(\exp\left(-\sqrt{\frac{i\omega}{D_2(0)}} x\right)\right) = \cos\left(\sqrt{\frac{\omega}{2D_2(0)}} x\right) \exp\left(-\sqrt{\frac{\omega}{2D_2(0)}} x\right)$
- $d_2 = \mathcal{I}m\left(\exp\left(-\sqrt{\frac{i\omega}{D_2(0)}} x\right)\right) = -\sin\left(\sqrt{\frac{\omega}{2D_2(0)}} x\right) \exp\left(-\sqrt{\frac{\omega}{2D_2(0)}} x\right)$
- $e_j = \mathcal{R}e\left(\frac{1}{p_j + \sqrt{i\omega D_j(0)}}\right) = \frac{p_j + \sqrt{\frac{D_j(0)\omega}{2}}}{p_j^2 + D_j(0)\omega + p_j\sqrt{2D_j(0)\omega}}$

$$\bullet f_j = \mathcal{I}m \left(\frac{1}{p_j + \sqrt{i\omega D_j(0)}} \right) = -\frac{\sqrt{\frac{D_j(0)\omega}{2}}}{p_j^2 + D_j(0)\omega + p_j \sqrt{2D_j(0)\omega}}$$

Thanks to these equalities we can recast \mathcal{K}_j in the following form:

$$\begin{aligned} \mathcal{K}_1 &= (e_1 + if_1) \left(1 - \sum_n (a_1 + ib_1) \Phi_{n,1}(0) \int_{-L_1}^0 \tilde{D}_1(x) \frac{d\Phi_{n,1}}{dx} (c_1(x) + id_1(x)) dx \right) \\ \mathcal{K}_2 &= (e_2 + if_2) \left(1 + \sum_n (a_2 + ib_2) \Phi_{n,2}(0) \int_0^{L_2} \tilde{D}_2(x) \frac{d\Phi_{n,2}}{dx} (c_2(x) + id_2(x)) dx \right) \end{aligned}$$

and by noting

$$\begin{aligned} g_1 &= \sum_n \left[a_1 \int_{-L_1}^0 \tilde{D}_1(x) \frac{d\Phi_{n,1}}{dx} c_1(x) dx - b_1 \int_{-L_1}^0 \tilde{D}_1(x) \frac{d\Phi_{n,1}}{dx} d_1(x) dx \right] \Phi_{n,1}(0) \\ h_1 &= \sum_n \left[b_1 \int_{-L_1}^0 \tilde{D}_1(x) \frac{d\Phi_{n,1}}{dx} c_1(x) dx + a_1 \int_{-L_1}^0 \tilde{D}_1(x) \frac{d\Phi_{n,1}}{dx} d_1(x) dx \right] \Phi_{n,1}(0) \\ g_2 &= \sum_n \left[a_2 \int_0^{L_2} \tilde{D}_2(x) \frac{d\Phi_{n,2}}{dx} c_2(x) dx - b_2 \int_0^{L_2} \tilde{D}_2(x) \frac{d\Phi_{n,2}}{dx} d_2(x) dx \right] \Phi_{n,2}(0) \\ h_2 &= \sum_n \left[b_2 \int_0^{L_2} \tilde{D}_2(x) \frac{d\Phi_{n,2}}{dx} c_2(x) dx + a_2 \int_0^{L_2} \tilde{D}_2(x) \frac{d\Phi_{n,2}}{dx} d_2(x) dx \right] \Phi_{n,2}(0) \end{aligned}$$

we obtain

$$\begin{aligned} \mathcal{K}_1 &= (e_1(1 - g_1) + f_1 h_1) + i(f_1(1 - g_1) - e_1 h_1) \\ \mathcal{K}_2 &= (e_2(1 + g_2) - f_2 h_2) + i(f_2(1 + g_2) + e_2 h_2) \end{aligned}$$

Hence the convergence factor ρ thanks to (1.39).

Contents

I	Introduction and model problem	3
1	Introduction	3
2	Model problem and Optimized Schwarz Methods	4
2.1	Formulation of global-in-time Schwarz method	5
2.2	Convergence of the algorithm	6
2.3	Optimized Schwarz Method	8
II	The constant coefficients case	9
3	Optimized Schwarz method with <i>Neumann-Robin</i> interface conditions	9
4	OSM for a diffusion problem with discontinuous (but constant) coefficients: two-sided Robin transmission conditions	12
4.1	Behaviour of the convergence factor with respect to the Robin parameters	13
4.2	Extrema of ρ_{RR} with respect to ζ	14
4.3	Equioscillation of ρ_{RR} at the end points	14
4.4	Solution of the minmax problem	16
4.5	The continuous case	21
5	Behaviour of Schwarz method with finite subdomains	23
5.1	Optimal symbols on bounded domains	23
5.2	Consequences for <i>Optimized Schwarz Methods</i>	26
III	The variable coefficients case	26
6	OSM for diffusion problems with spatially variable coefficients	26
6.1	Analytical determination of the shape of the errors	27
6.2	Convergence factor of the <i>Dirichlet-Neumann</i> algorithm with spatially variable coefficients	30
6.3	Convergence factor of the <i>Robin-Robin</i> algorithm with spatially variable coefficients	32
7	Numerical results	33
7.1	Discretization and initial conditions	33
7.2	Testcase # 1	34
7.3	Testcase # 2: parabolic diffusion profiles	38
8	Conclusion	40
A	Determination of the convergence rate in the case of variable coefficients	43



Centre de recherche INRIA Grenoble – Rhône-Alpes
655, avenue de l'Europe - 38334 Montbonnot Saint-Ismier (France)

Centre de recherche INRIA Bordeaux – Sud Ouest : Domaine Universitaire - 351, cours de la Libération - 33405 Talence Cedex
Centre de recherche INRIA Lille – Nord Europe : Parc Scientifique de la Haute Borne - 40, avenue Halley - 59650 Villeneuve d'Ascq
Centre de recherche INRIA Nancy – Grand Est : LORIA, Technopôle de Nancy-Brabois - Campus scientifique
615, rue du Jardin Botanique - BP 101 - 54602 Villers-lès-Nancy Cedex
Centre de recherche INRIA Paris – Rocquencourt : Domaine de Voluceau - Rocquencourt - BP 105 - 78153 Le Chesnay Cedex
Centre de recherche INRIA Rennes – Bretagne Atlantique : IRISA, Campus universitaire de Beaulieu - 35042 Rennes Cedex
Centre de recherche INRIA Saclay – Île-de-France : Parc Orsay Université - ZAC des Vignes : 4, rue Jacques Monod - 91893 Orsay Cedex
Centre de recherche INRIA Sophia Antipolis – Méditerranée : 2004, route des Lucioles - BP 93 - 06902 Sophia Antipolis Cedex

Éditeur
INRIA - Domaine de Voluceau - Rocquencourt, BP 105 - 78153 Le Chesnay Cedex (France)
<http://www.inria.fr>
ISSN 0249-6399